



Aftershock Sequences of the Recent Major Earthquakes in New Zealand

VLADIMIR G. KOSSOBOKOV^{1,2,3,4}  and ANASTASIA K. NEKRASOVA¹

Abstract—The three clusters of the epicenters of the nine recent (1993–2018) earthquakes of magnitude 7.0 or larger in New Zealand are located in three different tectonic environments of the Australia–Pacific Plate boundary, including the southern part of the Kermadec Trench (showing rapid westward subduction), the oblique collision zone between the Pacific Plate and Indo-Australian Plate with the dominant Alpine Fault (showing right-lateral strike-slip movement), and the Puysegur Trench (showing eastward oblique subduction). From the viewpoint of the unified scaling law for earthquakes (USLE), these regions are characterized by different levels of seismic rate (A), earthquake magnitude exponent (B), and fractal dimension of epicenter loci (C). The recent major earthquakes exemplify different scenarios of aftershock sequences in terms of either the dynamics of interevent time (τ) or the USLE control parameter ($\eta = \tau \times 10^{B \times (5-M)} \times L^C$), where τ is the time interval between two successive earthquakes, M is the magnitude of the second one, and L is the distance between them. We find the existence, in the long term, of different, intermittent levels of rather steady seismic activity characterized by near-constant values of mean η ($\langle \eta \rangle$), which, in the mid-term, switch between one another at times of critical transitions, including those associated with all but one magnitude 7.0 or larger earthquake. At such a transition, seismic activity may follow different scenarios with interevent time scaling of different kinds. Evidently, although these results based on analysis of an individual series do not support the presence of universality in seismic energy release, they provide constraints on modeling realistic seismic sequences for earthquake physicists and supply decision-makers with information for improving local seismic hazard assessments.

Key words: Unified scaling law for earthquakes, strong earthquakes, sequences of associated earthquakes, background seismic activity, self-organized nonlinear dynamical system, control parameter of a system.

1. Introduction

A coherent phenomenology on earthquakes and their consequences is still lacking due to the specifics of seismic observations, where the timing, location, and size of an event are estimated indirectly from seismographic records registered by a network of operational stations. Apparently, earthquakes occur through sporadic movement in highly stressed hierarchies of blocks and faults in the lithosphere of the Earth (Keilis-Borok 1990). However, seismic evidence indicates a wide range in the observed impulsive energy release. The amount of seismic energy of a detectable magnitude $M = -2$ earthquake is believed to be about 63 J (Storcheus 2011) and could be related to movement of an ensemble of tens of thousands of consolidated grains of rock, each about 10^{-3} m in size; on the other hand, the amount of seismic energy released in a single $M = 9$ megathrust rupture over a length of 700–1300 km amounts to more than 10^{18} J; e.g., the recent 26 December 2004 Sumatra–Andaman, $M_W = 9.3$ (Lay et al. 2005) and 11 March 2011 Tohoku $M_W = 9.1$ (Simons et al. 2011) megathrust events released energy of about 5.6×10^{18} J and 2.8×10^{18} J, respectively, while the energy of the largest, instrumentally recorded, 22 May 1960 Great Chilean, $M_W = 9.5$ earthquake (Kanamori and Cipar 1974) is about 11.2×10^{18} J, representing more than one-half of the total global seismic energy release in the 20th century (Di Giacomo and Bormann 2011).

Despite more than a century of instrumental observations, understanding the physics of seismic events remains complicated (Gardner and Knopoff 1974; Keilis-Borok 1990; Turcotte 1997; Davies 1999; Gabrielov et al. 1999; Kanamori and Brodsky 2001 and refs. therein). Some fundamental integral properties of seismic events are widely recognized in

¹ Institute of Earthquake Prediction Theory and Mathematical Geophysics, RAS, Moscow, Russian Federation. E-mail: volodya@mitp.ru

² Geophysical Center, RAS, Moscow, Russian Federation.

³ Institut de Physique du Globe de Paris, Paris, France.

⁴ International Seismic Safety Organization, Arsita, Italy.

literature, i.e., the Omori law in its original form (Omori 1894) or with slight modifications, the Gutenberg–Richter relationship (Gutenberg and Richter 1944, 1954), and the apparent fractal distribution of earthquake epicenters in space (Okubo and Aki 1987; Turcotte 1997). Given the complexity of this seismic reality, it is no surprise that the assumption of an analytically trackable model of earthquake recurrence requires data adjustment and, by necessity, leads to identification of main shocks along with hypothetical distributions of their size and interevent time, and the location of their fore- and aftershocks. As a result, some commonly accepted models based on unreliable estimates of earthquake return periods at a given site remain the basic source of erroneous seismic hazard assessments (Kossobokov and Nekrasova 2012; Wyss et al. 2012; Davis et al. 2012; Panza et al. 2014; Nekrasova et al. 2014; Kossobokov et al. 2015a).

Although the Omori law has elicited a long-lived controversy (Utsu et al. 1995) in seismology, where some events exhibit aftershocks whose number decays according to significantly different model functions while some do not have aftershocks at all, there is growing evidence that distributed seismicity in a wide range of magnitudes $M \in (M_-, M_+)$ and sizes $L \in (L_-, L_+)$ obeys the unified scaling law for earthquakes (USLE), generalizing the Gutenberg–Richter relation as follows:

$$\log_{10}N(M, L) = A + B \times (5 - M) + C \times \log_{10}L \quad (1)$$

where $N(M, L)$ is the expected annual number of earthquakes of magnitude M within an earthquake-prone area of diameter L ; A , B , and C are constants, where A and B characterize the annual rate of magnitude 5 events and the magnitude exponent, correspondingly, analogous to the a - and b -values in the Gutenberg–Richter relationship (Gutenberg and Richter 1944), and C estimates the fractal dimension d_f of the epicenter loci at the site (Nekrasova and Kosobokov 2005). The results of global and regional studies (Kossobokov and Mazhkenov 1994; Bak et al. 2002; Nekrasova and Kossobokov 2002, 2005, 2016; Nekrasova et al. 2011, 2015; Parvez et al. 2014) confirm the validity of the USLE at different scales of analysis, as well as in a dual formulation with the waiting times T between earthquakes with magnitude greater than M occurring within a range L (Bak et al. 2002; Christensen et al. 2002) instead of the rate of occurrence $N(M, L)$.

The nine earthquakes of magnitude 7.0 or larger that occurred in New Zealand from 1993 to 2018 (Table 1, Fig. 1) are located in three very different tectonic environments of the Australia–Pacific Plate boundary (Stirling et al. 2012). In particular, (1) the 1995/02/05, 2001/08/21, and 2016/09/01 events ruptured the southern part of rapid westward subduction

Table 1

The nine major earthquakes in New Zealand from 1993 to 2017

Origin time	Latitude	Longitude	Depth	M_{GeoNet}	M_{ANSS}	Index	Place ^a
1993/08/10 00:51:52	− 45.277	166.927	28	6.8	7.0	f	63.8 km WNW of Te Anau (2074) 166.7 km NW of Invercargill (47,287)
1995/02/05 22:51:02	− 37.759	178.752	21	7.2	7.1	a	118.9 km NNE of Gisborne (34,274)
2001/08/21 06:51:58	− 36.813	− 179.575	33	7.1	7.1	b	295.4 km NE of Gisborne (34,274)
2003/08/21 12:12:50	− 45.104	167.144	28	7.1	7.2	g	56.8 km NW of Te Anau (2074) 171.9 km NNW of Invercargill (47,287)
2004/11/22 20:26:32	− 46.676	164.721	10	7.0	7.1	h	255.5 km W of Riverton (1651) 280.0 km W of Invercargill (47,287)
2009/07/15 09:22:29	− 45.762	166.562	12	7.8	7.8	i	97.9 km WSW of Te Anau (2074) 155.4 km WNW of Invercargill (47,287)
2010/09/03 16:35:42	− 43.522	171.830	12	7.2	7.0	d	19.1 km NE of Methven (1236) 65.0 km W of Christchurch (363,926)
2016/09/01 16:37:55	− 37.359	179.146	19	7.1	7.0	c	175.2 km NE of Gisborne (34,274)
2016/11/13 11:02:56	− 42.737	173.054	15	7.8	7.8	e	54.4 km NNE of Amberley (1105) 94.8 km NNE of Christchurch (363,926)

^aDirection data from the ANSS Comprehensive Earthquake Catalog indicate the position of the event relative to the city (with population given in brackets)

beneath the Kermadec Trench, (2) those on 2010/09/03 and 2016/11/13 occurred within the segment of the complex system of blocks and faults of the oblique collision zone between the Pacific Plate and Indo-Australian Plate with the dominant Alpine Fault showing right-lateral strike-slip movement, and (3) the four events of 1993/08/10, 2003/08/21, 2004/11/22, and 2009/07/15 released major accumulated stresses beneath the Puysegur Trench showing eastward oblique subduction. The most recent, 13 November 2016 Kaikōura earthquake is a spectacular example that proves the occurrence of very complex

ruptures with diverse orientations, slip directions, and degrees of mechanical linkage involving numerous blocks and faults of the Earth lithosphere (Hamling et al. 2017). The earthquake epicenter is located about 20 km south of the Hope Fault, while its aftershocks extend along the Humps and Hundalee Faults for about 80 km offshore near Kaikōura, then step north along the Jordan Thrust and Kekerengu Fault. Their moment tensor determinations reveal a mixture of reverse and strike-slip mechanisms. The complexity of the rupture processes in the other major earthquakes of New Zealand is evident from

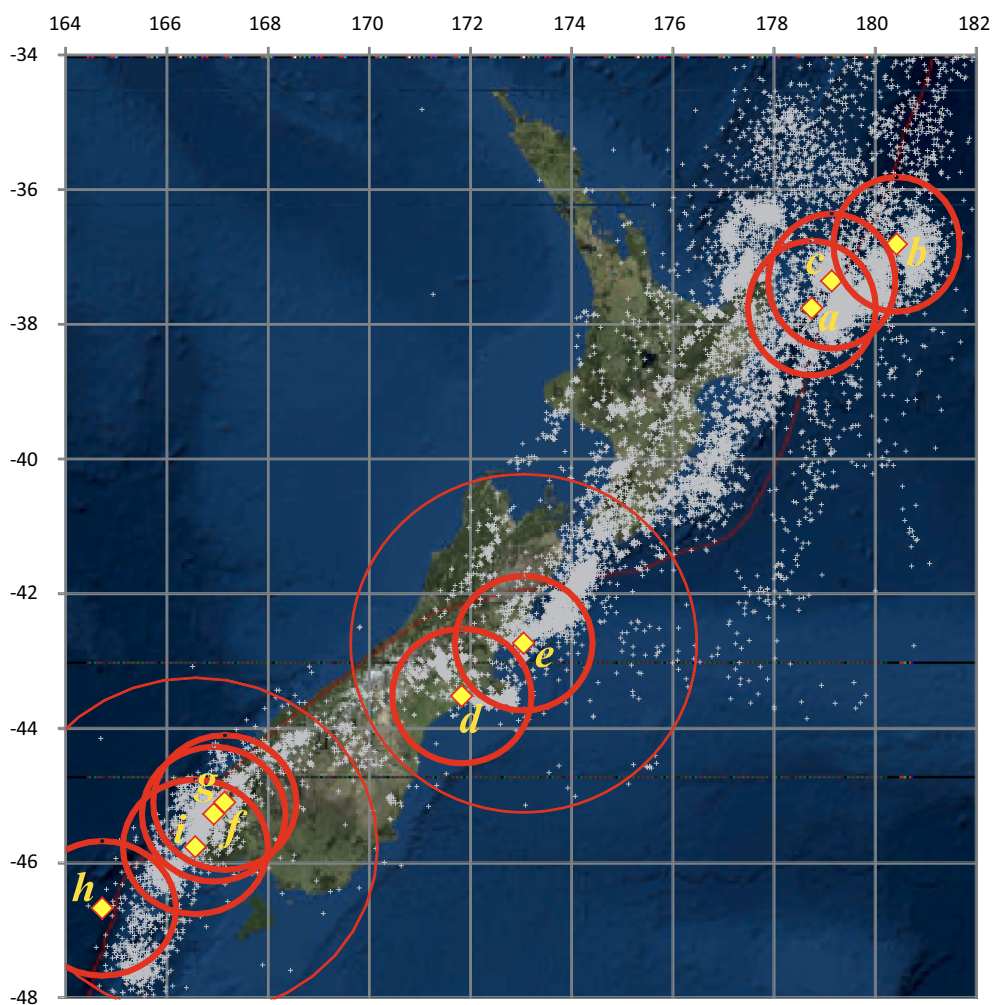
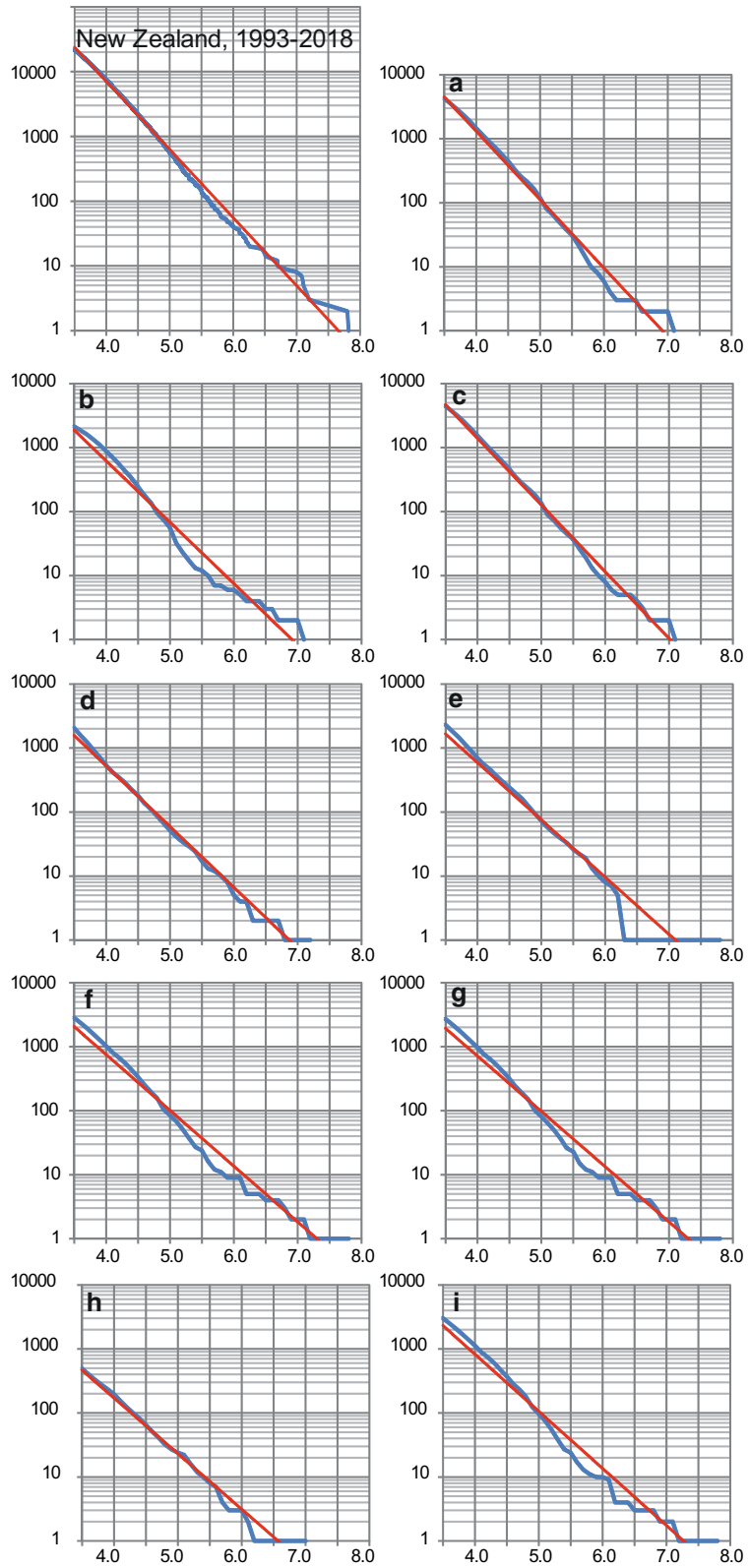


Figure 1

Epicenters of the nine major earthquakes (ANSS, 1993–2017; yellow diamonds with indices in circles of 1° radius) and earthquakes of magnitude 3.5 or above (GeoNet, 1993–2017; small grey crosses) in New Zealand. Note: indices correspond to Table 1 and follow chronological order within each of the three clusters; magnitude $M = 7.8$ earthquakes additionally encircled with $R = 2.5^\circ$ circles



◀Figure 2

Cumulative number of earthquakes above certain magnitude in New Zealand from 1993 to 2018 (blue) and its exponential trend line (red) in the study area and at an angular distance of 1° from the epicenters of the major earthquakes listed in Table 1

many multidisciplinary studies (e.g., Fry et al. 2009; Gledhill et al. 2010; Kaiser et al. 2012; Reyners et al. 2013). From the viewpoint of the USLE, these three segments of the Australia–Pacific Plate boundary are characterized by different levels of seismicity rate (A), earthquake magnitude exponent (B), and fractal dimension of epicenter loci (C) (Nekrasova and Kossobokov 2002). In the following, we investigate quantitatively the nearby seismic dynamics in advance and after these nine recent major earthquakes in terms of both the interevent time (τ) and the USLE control parameter [$\eta = \tau \times 10^{B \times (5-M)} \times L^C$], where τ is the time between two successive earthquakes, M is the magnitude of the second one, and L is the distance between them. (The USLE states that the distribution of interevent times depends only on the value of the variable η .)

2. Data

Seismicity of New Zealand from 01 January 1993 through 21 August 2018 is considered within 34° – 48° S and 164° – 182° E. According to Fig. 2, the online database of the official source of geological hazard information for New Zealand (GeoNet 2018) provides a reasonably complete record of earthquakes of magnitude 3.5 or above in the study area. (Note that the magnitude of completeness of the GeoNet catalog is about 2.5 or smaller in some inland territories of New Zealand.) For each of the total of 21,953 earthquakes considered in our study, the catalog reports the GeoNet official magnitude M (which is of the preferred moment magnitude type for large events and the local determination for the others). The Gutenberg–Richter plot for the total study area of New Zealand, i.e., the cumulative number of earthquakes of magnitude M or above, follows an exponential best-fit trend line with slope (b -value) of

1.03 and $R^2 = 0.993$. The plot is below its trend line in the magnitude range from 5 to 6.5, then rises above it.

According to the global ANSS Comprehensive Earthquake Catalog (ComCat 2017), nine major earthquakes of magnitude 7 or larger occurred (Table 1), with magnitudes and locations slightly different from those listed in the GeoNet database. The discrepancy of up to 0.2 lies quite within the natural intrinsic accuracy of earthquake magnitude determinations. The Gutenberg–Richter plots for the circles nearby the epicenters of the nine major earthquakes (Fig. 2a–i) follow exponential best-fit trend lines with b -values from 0.86 to 1.07 and R^2 ranging from 0.951 to 0.993. Figure 3 shows three-dimensional (3-D) plots of the earthquake distribution by magnitude (top) and latitude (bottom) versus time.

2.1. Interevent Times and Their Moving Average

We calculate the interevent times (τ , in days) and plot them versus the origin time along with the 50-event moving-average trend line ($\langle \tau \rangle$, red curve) for both the entire study area (Fig. 4) and the three nonoverlapping subregions (Fig. 5) defined by latitude ranges as follows: southern Kermadec Trench from 34.0° S to 38.7° S, oblique collision zone between the Pacific and Indo-Australian Plates from 38.7° S to 43.7° S, and Puysegur Trench from 43.7° S to 48.0° S. Visual inspection of Figs. 3, 4, 5 reveals clustered irregularity of the seismic dynamics in the study area. For all but the 2004 major earthquake that occurred 280 km west of Invercargill, there are rich series of associated events.

2.2. Foreshocks and Aftershocks

We now zoom in to nearby the nine major earthquakes for better resolution of the seismicity in space (Fig. 6) and time (Fig. 7):

The three major events in the Kermadec Trench (Fig. 6a–c), although of about the same magnitude, differ in their area and number of aftershocks in the first 128 days after the main shock (i.e., 2276, 962, and 344 earthquakes of magnitude 3.5 or larger, respectively); Note, however, that the southwestern wing of the 2001 series occurred after the 21 October

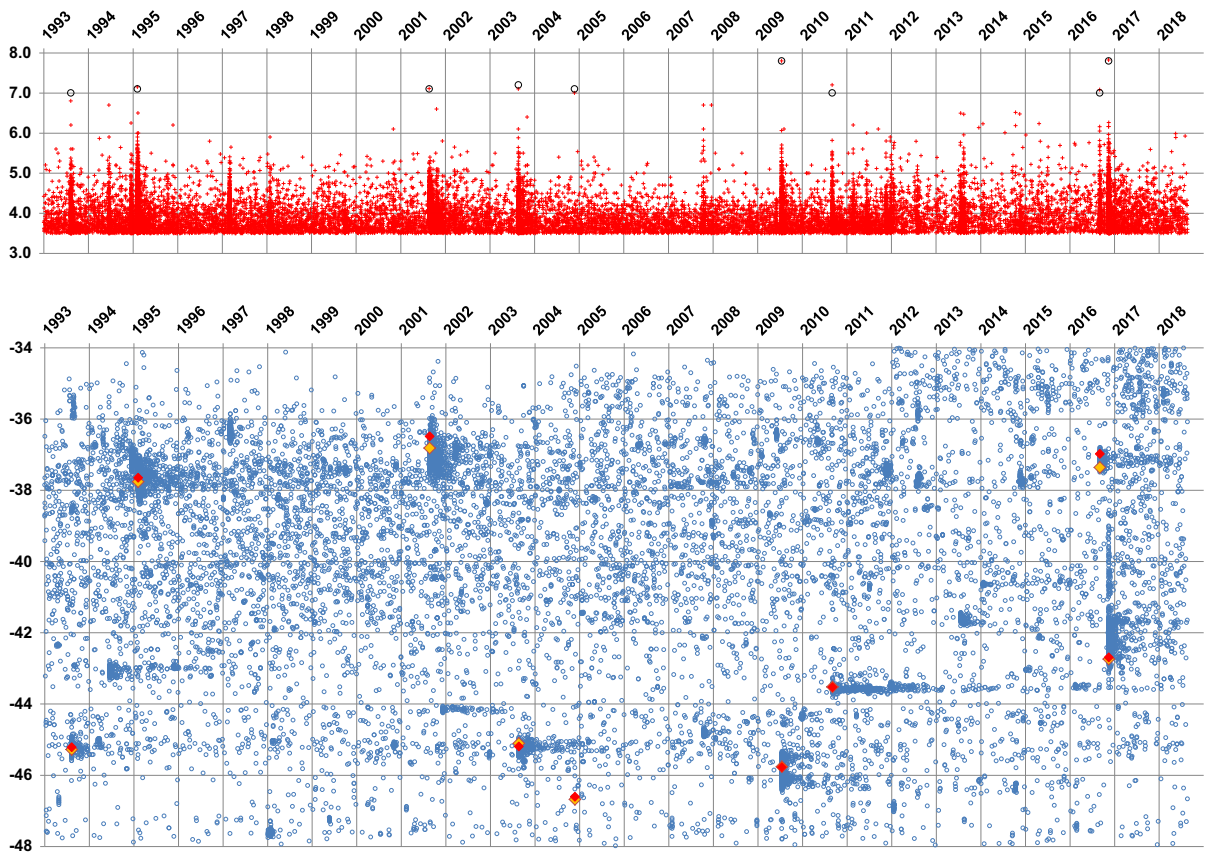


Figure 3

Magnitude–latitude–time distribution of earthquakes in New Zealand, 1993–2017. Notes: the ANSS magnitudes of the nine major earthquakes are given as open circles (top frame); red and yellow diamonds (bottom frame) mark the epicenters as determined by GeoNet and ANSS, respectively

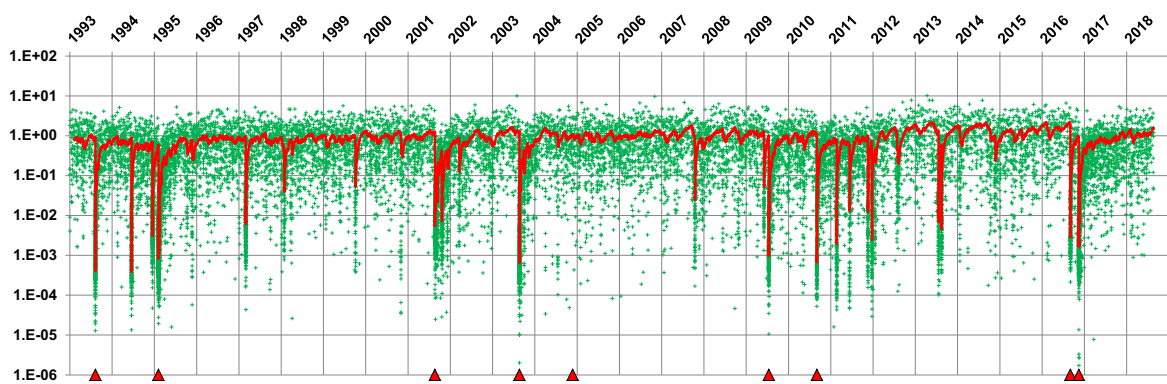


Figure 4

Intervent time (τ , in days) versus earthquake origin time in New Zealand (1993–2017). Note: the origin times of the nine major earthquakes are marked with red triangles on the origin time scale; red line is the moving average per 50 events ($\langle \tau \rangle$)

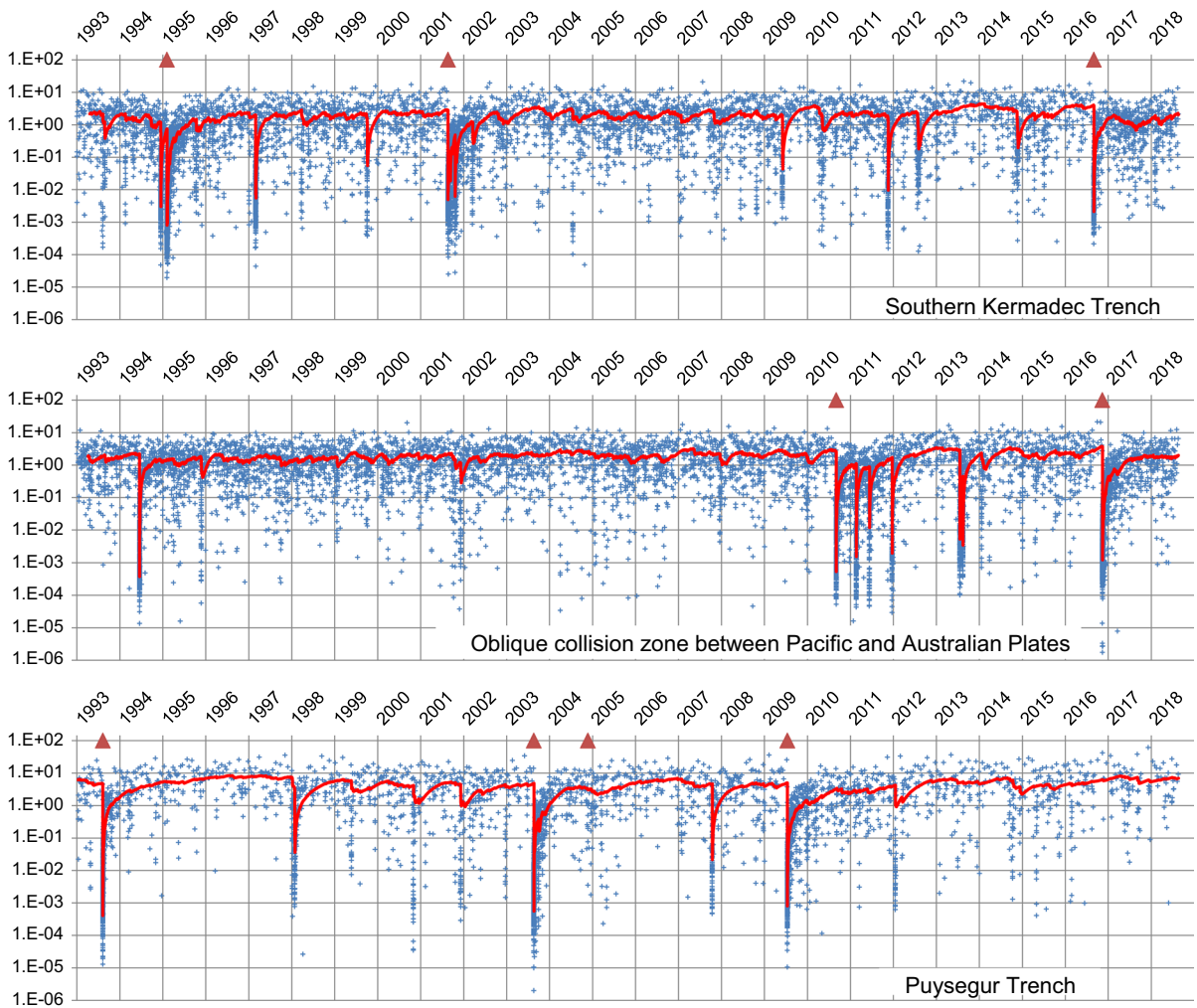


Figure 5

Interevent time (τ , in days) versus earthquake origin time in the three subregions of New Zealand (1993–2017). Same as in Fig. 4

2001, $M6.6$ earthquake, 2 months after the major shock on 21 August. The aftershock area of the two major earthquakes in the oblique collision segment of the Australia–Pacific Plate boundary (Fig. 6d, e) is in good agreement with scaling proportional to 10^M : the aftershock area of the 2010, $M7.0$ event (512 events) is about 6 times smaller than that of the 2016, $M7.8$ one (799 events). Moreover, as mentioned in “Introduction” section, the aftershocks of the 2016 earthquake step north from offshore near Kaikōura, surpassing the angular distance of 1° from the epicenter. In the region of the Puysegur Trench (Fig. 6f–i), the aftershock areas of the 1993, $M7.0$

and 2003, $M7.2$ major events (with 572 and 780 aftershocks) are about the same, whereas the major 2004 event with $M7.1$ was followed nearby by a series of only 15 earthquakes of magnitude 3.5 or larger within 128 days; the epicenters of the 721 aftershocks of the 2009, $M7.8$ major earthquake (Fig. 6i) are located within a region twice as large as the areas of the aftershocks after either the 1993, $M7.0$ or the 2003, $M7.2$ event, and compare well with the area and number of aftershocks after the 13 November 2016, $M7.8$ earthquake in the oblique collision zone between the Pacific and Indo-Australian Plates (Fig. 6e). The characteristics of the

seismicity nearby the nine major earthquakes are summarized in Table 2.

The choice of the space–time limits (angular distance of 1° from the epicenter and 128 days before and after the main shock origin time) as well as the choice of 50 events for the moving average of the interevent time (τ) are somewhat arbitrary. However, these are (1) in agreement with scaling of earthquake source parameters (e.g., Wells and Coppersmith 1994; Goda et al. 2016 and refs therein), (2) allow for statistics from nonoverlapping space–time volumes, (3) apparently catch patterns of nearby seismic dynamics, and (4) according to extensive stability

Figure 7

Interevent time (τ , in days) versus the origin time of the earthquakes occurring at angular distance of 1° from a main shock epicenter within ± 128 days from the main shock origin time for each of the nine major earthquake series in New Zealand, 1993–2018. Notes: red line is 50-event moving average ($\langle \tau \rangle$); the last plot (bottom right) compares the moving averages for the nine major earthquake series

checking with other choices of fixed limits, provide quantitative estimates for reliable qualitatively stable conclusions. Section 4 exemplifies a kind of stability check with a spatial limit of 2.5° from the epicenters for the two $M7.8$ earthquakes.

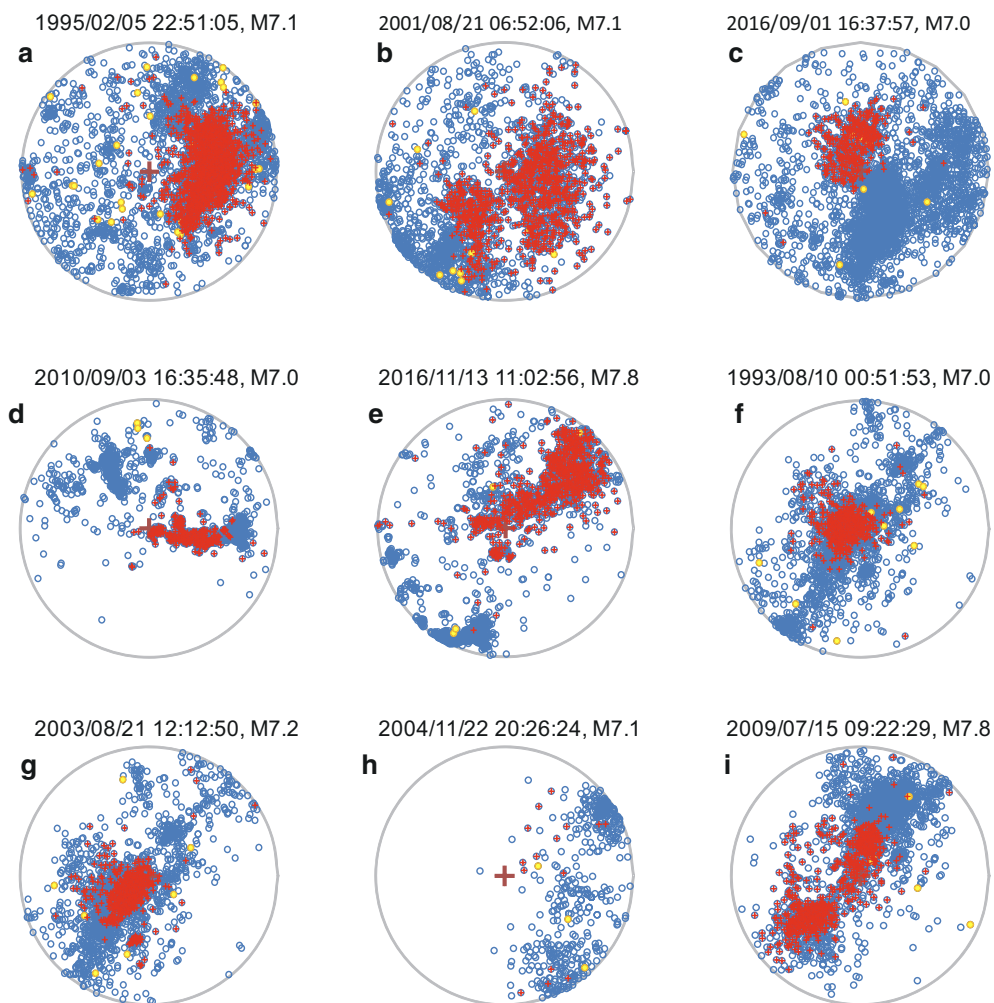


Figure 6

Epicenters of earthquakes at angular distance of 1° from the epicenter of each of the nine major earthquakes in New Zealand. Note: epicenters of earthquakes in 1993–2018 (open blue circles), and those occurring 128 days before (yellow circles) or 128 days after (small red crosses) the origin time of a major event

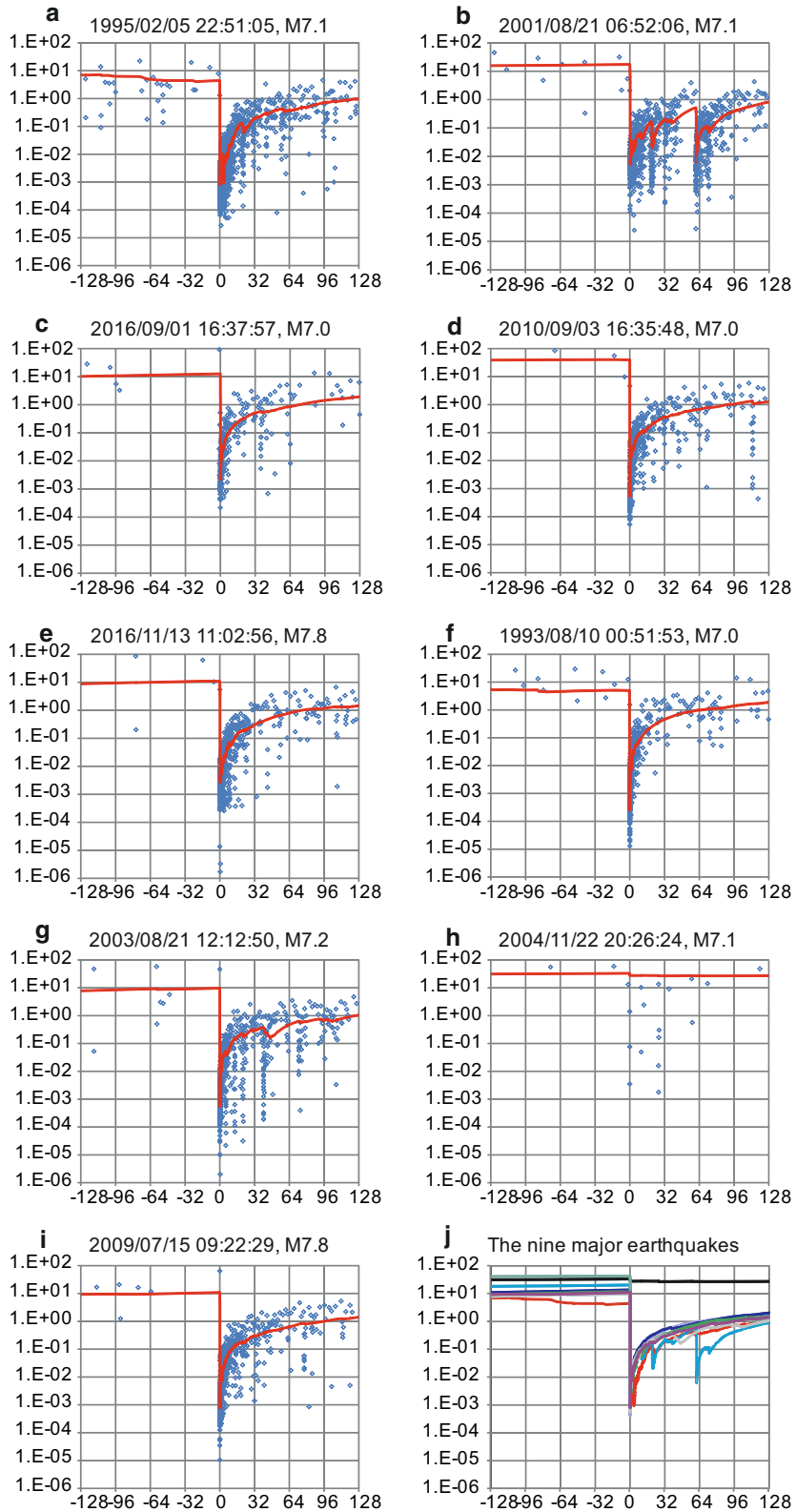


Table 2
Characteristics of the nine major earthquake series in New Zealand, 1993–2018

Index	Date	M_{ANSS}	A	B	C	N_f	N_a	M_{lf}	τ_{lf} (days)	D_{lf} (km)
a	1995/02/05	7.1	− 0.01	1.12	1.19	28	2276	4.3	1.31	110
b	2001/08/21	7.1	− 0.22	1.18	1.14	10	962	3.5	2.06	103
c	2016/09/01	7.0	− 0.19	0.97	1.19	11	344	3.7	0.52	24
d	2010/09/03	7.0	− 0.85	0.68	1.15	3	512	3.8	4.67	87
e	2016/11/13	7.8	− 0.80	0.65	1.22	4	799	4.0	5.48	105
f	1993/08/10	7.0	− 0.69	0.70	0.90	9	572	3.6	1.52	99
g	2003/08/21	7.2	− 0.81	0.61	0.89	7	780	3.8	46.33	96
h	2004/11/22	7.1	− 0.71	0.69	0.92	3	15	3.7	1.39	67
i	2009/07/15	7.8	− 0.81	0.61	0.89	5	721	3.8	63.36	51

Index refers to the corresponding plates in Fig. 6; A , B , and C are the USLE coefficients at the epicenter; N_f and N_a are the number of earthquakes of $M = 3.5$ or larger within 128 days before and after the main shock at angular distance of 1° from its epicenter, respectively; M_{lf} is the magnitude of the last foreshock of $M = 3.5$ or larger; τ_{lf} is the advance time to the main shock and D_{lf} is the distance to its epicenter

There are a moderate number of earthquakes preceding each of the nine major earthquakes in New Zealand; their epicenters are marked with yellow circles in Fig. 6, and their times are negative in Fig. 7. Although five of them occurred within about 2 days or less before a major earthquake, their distance to the incipient epicenter, except for the recent 1 September 2016, $M7.0$ event in the Kermadec Trench, is more than 66 km (Table 2), which might be too far to be attributed as “immediate foreshocks.” In the exceptional case, the advance time and distance were 0.517 days and 24 km, respectively. On the other hand, the commonly accepted radius of the preparation zone for a magnitude 7 earthquake (Dobrovolsky et al. 1979) is much larger than the angular distance of 1° considered here and compares to two-thirds of the entire extent of New Zealand; therefore, it is evident that each of the nine major earthquakes were preceded by some intermediate to short-term foreshocks in the magnitude range above 3.5. However, an observable rise of the 50-event moving average is evident only for one series, preceding the 5 February 1995, $M7.1$ main shock (Fig. 7a, j), whose series is also characterized by the largest number of aftershocks (2276; Table 2).

2.3. Modeling the Aftershock Decay

As mentioned above, the series of aftershocks of the nine major earthquakes in New Zealand differ in their area, shape, size, and number of shocks, and

thus not surprisingly, also in terms of their dynamics. Figure 7j enables easy comparison and reveals an evidently wide variety of the moving average of τ in the aftershock series following the nine major earthquakes. The empirical distribution functions for τ for each of the nine aftershock series plotted in Fig. 8 confirm this rather vivid variety.

Table 3 presents the Akaike information criterion (AIC 1974) values obtained using the SASeis AFT program (Utsu and Ogata 1997) for modeling the best fit of the aftershock rate decay. The rise of the interevent time is dual to the decay of the aftershock number, allowing for an additional model comparison of eight out of the nine series. Table 4 (columns τ) sums up the best-fit approximations of the 50-event moving average of the interevent time for each of the aftershock series within a few months (specifically, 128 days) after the main shock under the assumption of a linear or power-law rise. The minimum AIC values in Table 3 and the maximum R^2 values in Table 4 (columns τ) help to describe quantitatively the diversity of seismic activity decay scenarios after the major earthquakes in New Zealand. In fact, the AIC values for the classical Omori law are not that different from the best-fit choices in Table 3. The dual equivalent of the Omori law, i.e., a linear rise of the interevent time average ($\langle\tau\rangle$), outperforms the competing power law in six out of the eight cases in Table 4. Moreover, it is notable that the value of b in the power law is about 1 in all eight cases, except for the 2001 series of aftershocks ($b = 0.58$).

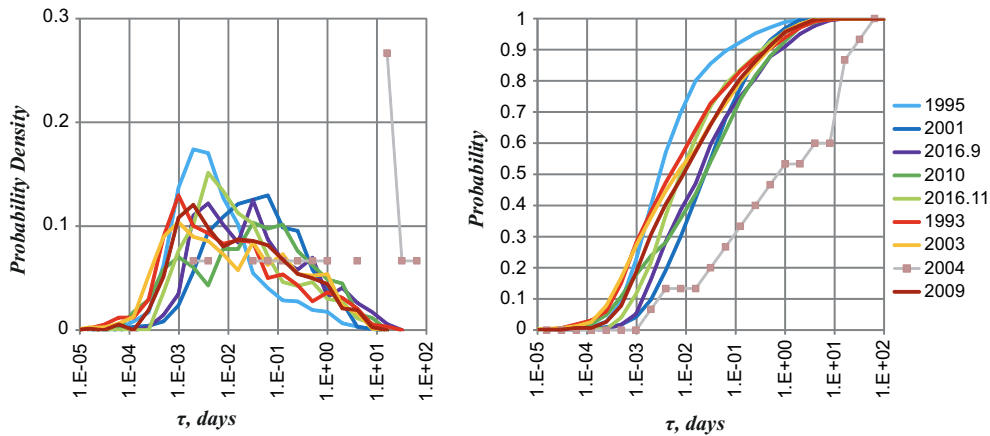


Figure 8

Empirical density (left) and cumulative (right) distribution functions of interevent time (τ , in days) in the aftershock series of the nine major earthquakes. Note the logarithmic time scale and bins exponentially increasing by factor 2

Table 3

The AIC values for the best fit of the rate of aftershock occurrence at time t , $f_i(t)$, after the major main shocks in New Zealand, 1993–2017

Date	$f_1(t)$	$f_2(t)$	$f_3(t)$	$f_4(t)$	$f_5(t)$	$f_6(t)$	$f_7(t)$	$f_8(t)$
05/02/1995	- 25,300	- 24,488	- 25,312	- 25,052	- 25,147	- 25,310	- 25,537	- 25,555
21/08/2001	- 3250	- 3316	- 3329	- 3289	- 2390	- 3309	- 4007	na
01/09/2016	- 3079	- 3308	- 3327	- 3320	- 3342	- 3341	- 3322	- 3317
03/09/2010	- 4630	- 4934	- 4965	- 5017	- 4932	- 5006	na	na
13/11/2016	- 8252	- 8130	- 8312	- 8177	- 8266	- 8310	- 8319	na
10/08/1993	- 7211	- 7504	- 7595	- 7493	- 7613	- 7589	na	na
21/08/2003	- 9376	- 9934	- 9932	- 9782	- 9922	- 9931	- 1002	- 10041
22/11/2004	na	na	na	na	na	na	na	na
21/08/2009	- 6559	- 6889	- 6893	- 6842	- 6746	- 6892	- 6895	na

$f_1(t) = B + K \exp(-qt)$ —exponential decay; $f_2(t) = B + K/(t + c)$ —exponential decay; $f_2(t) = B + K/(t + c)$ —Omori formula

$f_3(t) = B + K/(t + c)^p$ —modified Omori formula

$f_4(t) = B + K t^{b-1} \exp(-a t^b)$ —stretched exponent (Weibull distribution)

$f_5(t) = B + K \exp(-qt)/(t + c)$ —Otsuka formula

$f_6(t) = B + K \exp(-qt)/(t + c)^p$ —modified Otsuka formula

$f_7(t) = B + K/(t + c)^p + K_2/(t - T_2 + c_2)^p (K_2 = 0 \text{ for } t < T_2)$ —modified Omori model with second aftershock sequence starting at time T_2

$f_8(t) = B + K/(t + c)^p + K_2/(t - T_2 + c_2)^p + K_3/(t - T_3 + c_3)^p (K_2 = 0 \text{ for } t < T_2, \text{ and } K_3 = 0 \text{ for } t < T_3)$ —modified Omori model with second and third aftershock sequences starting at times T_2 and T_3 , respectively (Utsu and Ogata 1997)

The lowest “best fit” values are highlighted (bold)

3. Application of the USLE Control Parameter

Let us investigate the earthquake series by applying the USLE control parameter η , making use of the coefficients mapped on a global scale with resolution of 0.5° (Nekrasova and Kossobokov 2002). The maps of A , B , and C estimates nearby New

Zealand are shown in Fig. 9 (the values at the locations of major earthquakes are listed in Table 2). The southern part of the Kermadec Trench showing rapid westward subduction is characterized by the highest level of earthquake rate compared with the other two considered segments of the complex Australia–Pacific Plate boundary. The oblique collision zone

Table 4

The best fit approximations of the per 50 event moving average of inter-event time τ (columns $\langle\tau\rangle$) and USLE control parameter η (columns $\langle\eta\rangle$) during the first 128 days after the major main shock

	$\langle\tau\rangle$		$\langle\eta\rangle$	
	Linear $at + b$	Power at^b	Linear $at + b$	Power at^b
1995/02/05				
a	0.0070	0.0026	20.73	5.33
b	- 0.0196	0.9093	- 64.53	1.02
R^2	97.20%	77.98%	94.82%	82.02%
2001/08/21				
a	0.0030	0.0120	7.62	8.94
b	0.0132	0.5793	- 6.12	0.86
R^2	43.89%	56.80%	49.36%	71.07%
2016/09/01				
a	0.0145	0.0140	10.74	10.71
b	- 0.0031	0.9897	- 0.71	0.99
R^2	99.61%	99.60%	95.66%	98.57%
2010/09/03				
a	0.0106	0.0126	5.75	4.91
b	- 0.0020	0.934	- 6.60	1.02
R^2	99.41%	99.40%	98.43%	99.14%
2016/11/13				
a	0.0120	0.0060	8.35	4.90
b	- 0.0217	1.0716	- 5.22	1.11
R^2	98.88%	96.35%	96.48%	98.51%
1993/08/10				
a	0.0149	0.0107	1.88	0.96
b	- 0.0073	1.0197	- 1.71	1.09
R^2	99.65%	99.16%	98.91%	98.95%
2003/08/21				
a	0.0072	0.0090	0.82	0.78
b	0.0078	0.9608	- 0.32	0.98
R^2	95.93%	99.12%	91.88%	99.41%
2004/11/22				
na				
2009/07/15				
a	0.0104	0.0086	1.55	1.09
b	- 0.0097	0.9936	- 1.17	1.08
R^2	99.47%	98.46%	98.64%	99.07%

The model approximations with R^2 above 95% are highlighted (italics), for each main shock the largest values of R^2 are given in bold

between the Pacific and Indo-Australian Plates with the dominant Alpine Fault shows the lowest values of A , which correspond to about one or fewer earthquakes of magnitude 5 per 10 years on a $1^\circ \times 1^\circ$ area prone to earthquakes. The magnitude exponent parameter B highlights the Kermadec Trench segment with values above 1, while ranging from about 0.6 to 0.7 over the entire New Zealand Islands and the Puysegur Trench. The values of the fractal dimension of epicenter loci ($C > 1.1$) confirm the highly fractured zone of fast subduction down to latitude 42°S

and a dominating linear pattern of faulting ($C \approx 1$) to the south of it.

Figure 10 shows plots of the control parameter values $\eta = \tau \times 10^{B \times (5-M)} \times L^C$ versus the origin time for earthquakes at angular distance of 1° from the epicenter of each of the nine major earthquakes in New Zealand. The empirical distribution functions of η for each of the nine circles of radius 1° centered at the epicenters of the major earthquakes plotted in Fig. 11 confirm a wide spread over about five or more decimal orders of the bulk density distribution of η

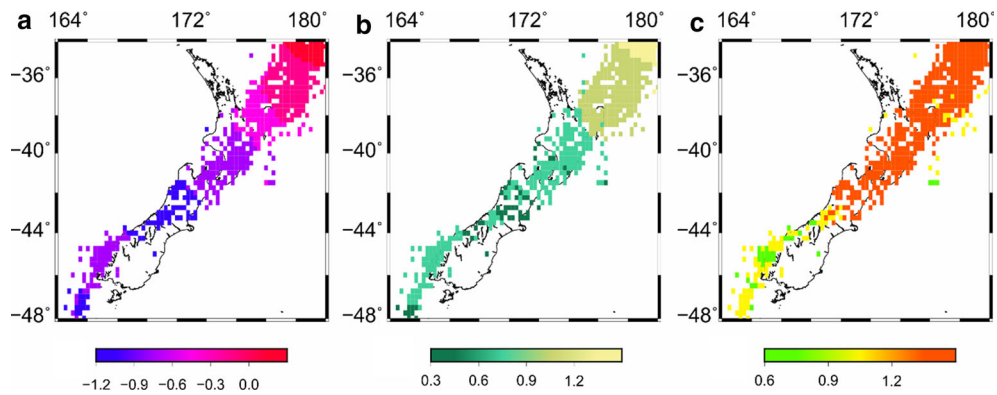


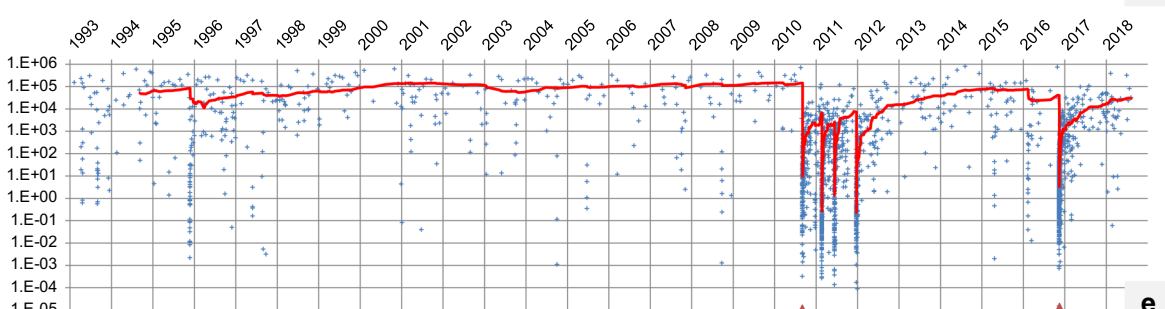
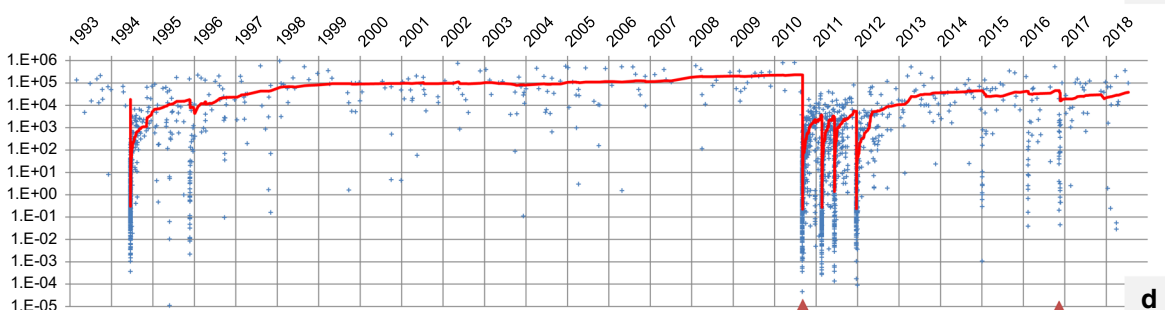
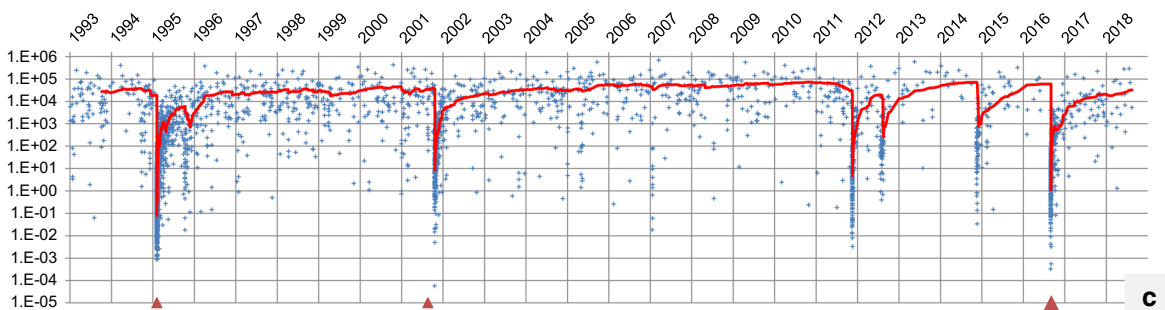
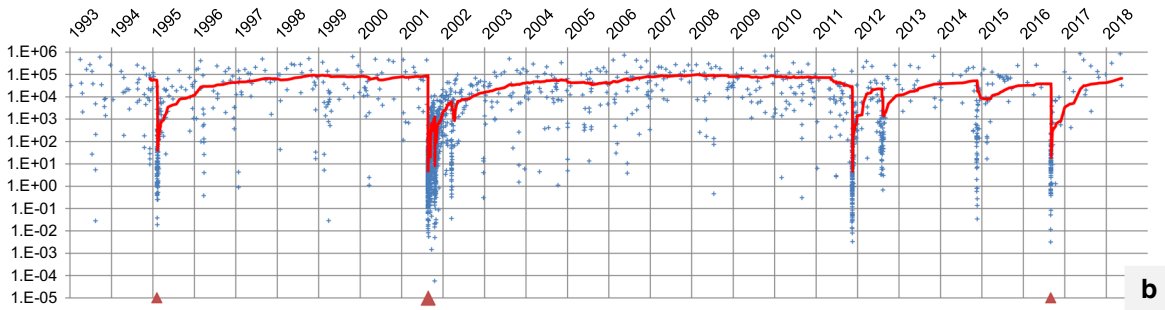
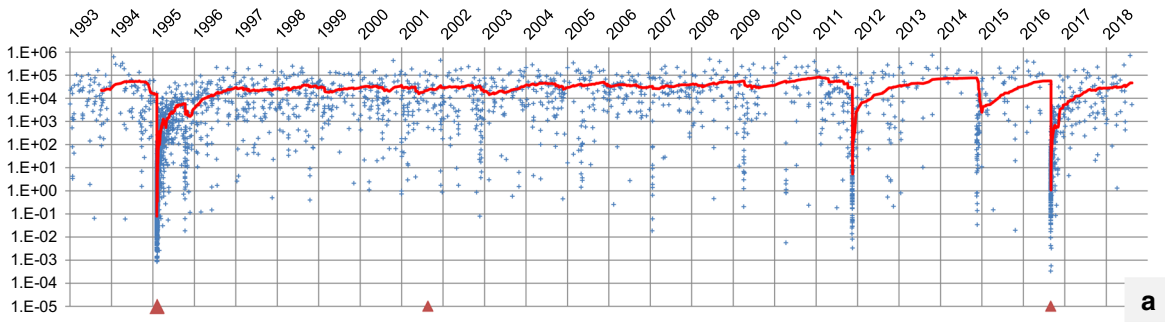
Figure 9
USLE coefficients nearby New Zealand (after Nekrasova and Kossobokov 2002)

and the variety of evidently different probability distributions; even for overlapping circles from the same cluster, the difference is impressive. Except for the two major earthquakes on 1993/08/10 and 2003/08/21 with epicenters at 26 km from each other, the difference is significant, with confidence above 99.9 % according to the nonparametric two-sample Kolmogorov–Smirnov statistic, λ_{KS} (Smirnov 1948; Kossobokov et al. 2008); in the exceptional case, the confidence of 85.8 % is less than commonly accepted levels, thus the hypothesis of the same distribution of η in the two largely overlapping circles cannot be rejected.

Naturally, the moving averages of η per 50 events ($\langle \eta \rangle$), red lines in Fig. 10) look similar for events of the same cluster due to the significant overlap of the circles considered (i.e., 72.4, 36.4, and 82.7 % of the total number of earthquakes of $M3.5$ or larger in the clusters of circles in the southern Kermadec Trench, oblique collision zone between Pacific and Australian Plates, and Puysegur Trench, respectfully). The plots of η and τ in a corresponding cluster (Figs. 10 and 5, respectively) look similar as well. In fact, the relationship between η and τ appears nonlinear. The best-fit approximation of τ as a function of η in all nine circles considered is the power law $\tau = a\eta^b$, characterized by b values of about 0.7–0.8 and R^2 above 80 % (Table 5). Therefore, the choice of the best-fit approximation of the 50-event moving average of the USLE control parameter (η) as a function of time since the origin time of the main shock (Table 4, columns $\langle \eta \rangle$) is qualitatively not that different from

those based on the interevent time τ (Table 4), although, formally, in contrast, the power-law fit of the η moving average outperforms the linear fit in six out of eight cases and the values of the power b are somewhat higher than those for the rise of τ . It should be noted, however, that (1) the quality of either the linear or power-law best-fit approximation of τ and η is almost equally good or bad, and (2) the b -values of the best-fit power law for all nine series of $\langle \eta \rangle$ lie in range from 0.86 to 1.11, i.e., well in agreement with the classical Omori (1894) law.

By inspection of Figs. 4, 5, and 10, one can find times of near-flat portions of the graphs where the moving averages change within one decimal order. Let us define the *periods of stability* by the condition that $\{t: \langle \eta \rangle(t) \text{ is larger than } \langle \eta \rangle_{\max}/10\}$, where $\langle \eta \rangle_{\max}$ is the maximal value of $\langle \eta \rangle$ over the entire time period considered. These periods of stability characterized by a low rate of seismicity are interrupted by comparatively short bursts of activity, most of them associated with the origin times of major earthquakes and their aftershocks. In particular, in Fig. 10a, the moving average of η fluctuates between 10^4 and 10^5 for about 90 % of time, which is a typical duration of the periods of stability for the nine major earthquakes in New Zealand (Table 6). It should be noted that the mean value of $\langle \eta \rangle$ and its error of determination, $\text{err}(\langle \eta \rangle) = \text{stdev}(\langle \eta \rangle)/\text{sqrt}(n)$, where n is the sample size, cannot be used for a straightforward comparison of the control parameter levels in different periods of stability due to the extremely wide spread of the bulk distribution of the values of η evident from Fig. 11.



◀Figure 10

USLE control parameter η versus earthquake origin time nearby the epicenters of the nine major earthquakes in New Zealand, 1993–2018. Notes: the origin times of the nine major earthquakes are marked with red triangles on the origin time scale; red line is the moving average of η per 50 events ($\langle\eta\rangle$)

Except for the last periods of stability nearby the epicenters of the nine major earthquakes, whose durations and estimates of the level of $\langle\eta\rangle$ may change in the future, Table 6 does not include the short ones that lasted for less than a year. To avoid using main-shock contributions to the moving average of η , the periods of stability terminate at the origin time of the last event in a series preceding each

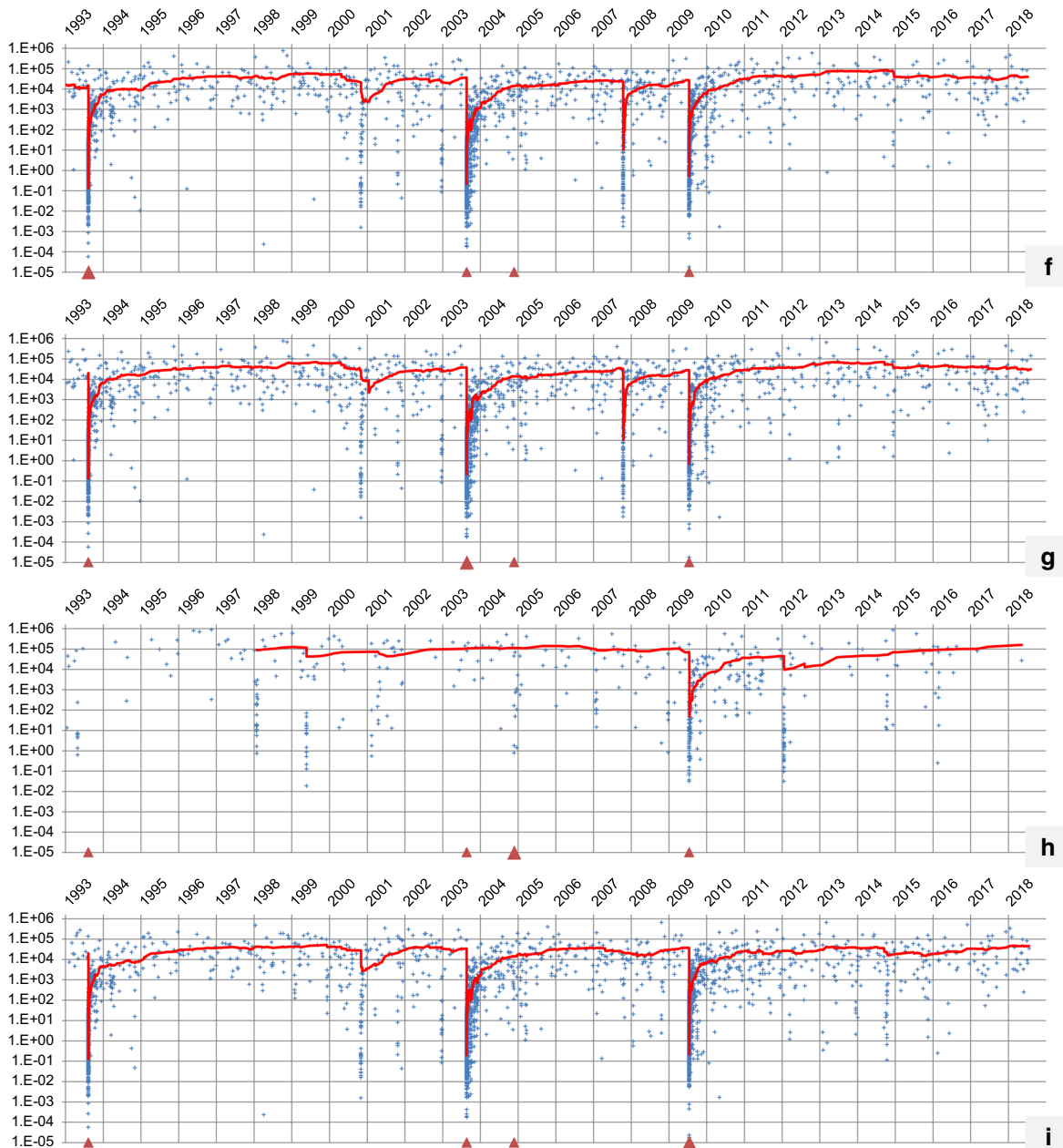


Table 5

Power-law approximations $\tau = a\eta^b$ nearby the nine major earthquakes in New Zealand, 1993–2018

Index	Date	a	b	R^2 (%)
a	1995/02/05	0.0035	0.7126	87.85
b	2001/08/21	0.0059	0.6919	85.14
c	2016/09/01	0.0045	0.7307	87.85
d	2010/09/03	0.0182	0.7445	89.50
e	2016/11/13	0.0136	0.7058	83.54
f	1993/08/10	0.0180	0.8056	92.68
g	2003/08/21	0.0232	0.8049	93.43
h	2004/11/22	0.0396	0.7280	88.42
i	2009/07/15	0.0194	0.8254	92.96

of the major main shocks. In particular, Table 6 provides the three estimates for the three connected periods of stability in the neighborhood of the 22 November 2004, $M = 7.1$ major earthquake whose occurrence did not produce any noticeable aftershock series that would interrupt the 10.81-year period of stability with $\langle\eta\rangle = 72.88$ [$\text{err}(\langle\eta\rangle) = 1.87$]; specifically, we distinguish the 6.17 years before the main shock ($\langle\eta\rangle = 69.29$), 2.19 years to the 50th earthquake after the main shock ($\langle\eta\rangle = 80.55$), and 2.40 years interrupted by widespread activation after the 15 July 2009, $M = 7.8$ earthquake ($\langle\eta\rangle = 73.00$).

The 42 periods of stability identified in Table 6 are characterized by apparently different levels of η . Out of the total of 34 cases in the nine areas considered, the level of $\langle\eta\rangle$ is either higher by a factor of 1.25 than that of the previous (in 8 cases), or lower (in 16 cases), or changes within 80–120 % (in the other 10 cases).

Except for the 22 November 2004, $M = 7.1$ earthquake, a major main shock interrupted a period of stability and was followed after a delay (ranging from 112 days after the 15 July 2009, $M = 7.8$ to 959 days after the 3 September 2010, $M = 7.0$ earthquake) by a lower level of $\langle\eta\rangle$ in four cases (i.e., the 21 August 2003 $M = 7.2$, 03 September 2010, $M = 7.0$, 01 September 2016, the $M = 7.0$, and 13 November 2016, $M = 7.8$ earthquakes), by a higher level in only one case (the 10 August 1993, $M = 7.0$ earthquake), and remained about the same (i.e., within 80–120 % of the previous level) in the other four cases (Table 7, where $\langle\eta\rangle_a/\langle\eta\rangle_b > 1.25$ given in italics and $\langle\eta\rangle_a/\langle\eta\rangle_b < 0.80$ given in bold). Thus, the

major earthquakes in New Zealand changed, eventually, the seismic regime nearby their locations four times to a higher and once to a lower rate of earthquake occurrence, while returning back to about the same rate in the other four cases.

4. The Two $M 7.8$ Cases: the 2009 Dusky Sound and 2016 Kaikōura Earthquakes

Seven out of the nine major earthquakes in New Zealand belong to about the same magnitude range from 6.8 to 7.2 (Table 1), which is within the intrinsic accuracy of an earthquake magnitude determination of about 0.2–0.3 units (Gutenberg and Richter 1944; Harte and Vere-Jones 1999; Kagan 2003; Werner and Sornette 2008). On the other hand, the two largest, i.e. the 15 July 2009 Dusky Sound (Fry et al. 2009) and 13 November 2016 Kaikōura (Hamling et al. 2017) earthquakes are both of magnitude $M_W = 7.8$, a size that may require a larger definition of nearby area for adequate assessment of the seismic dynamics in advance and after their occurrence. In particular, as mentioned in Sect. 2.2, for the 2016 Kaikōura earthquake, the angular distance of 1° from the epicenter is insufficient to capture the entire set of its evident aftershocks. Therefore, let us increase the circle of investigation in proportion to source size scaling (Goda et al. 2016), and change their common radius from 1° to become $1^\circ \times 10^{0.5 \times (7.8 - 7.0)} = 2.51^\circ$, i.e., 279 km from the epicenter of the main shock.

Table 6

Periods of stability of the control parameter η nearby epicenters of the nine major earthquakes in New Zealand region

Major earthquake	Start time	End time	Duration, years	Level of $\langle \eta \rangle \pm \text{err}(\langle \eta \rangle)$	
1995/02/05 22:51:02, $M = 7.1$	1993/10/04 15:02:20	1995/02/04 15:25:31	1.34	39.47 \pm 1.68	
			1.10		
	1996/03/12 03:16:51	2011/11/18 07:46:54	15.69	31.52 \pm 0.36	
	2012/04/09 21:25:44	2014/12/13 01:16:14	2.68	43.13 \pm 1.94	
	2015/06/05 13:27:03	2016/09/01 04:13:05	1.24	33.66 \pm 2.52	
2001/08/21 06:51:58, $M = 7.1$	2017/03/08 04:35:19	<i>2018/08/17 04:47:03</i>	<i>1.44</i>	22.92 \pm 0.99	
	1995/11/21 22:19:13	2001/08/19 05:20:25	5.74	61.04 \pm 2.02	
			1.08		
	2002/09/20 14:16:46	2011/11/18 04:14:18	9.16	53.97 \pm 1.33	
	2012/11/28 09:46:47	2014/11/13 19:25:45	1.96	32.24 \pm 2.83	
	2015/04/02 07:19:01	2016/06/08 09:12:54	1.19	22.81 \pm 1.85	
	2017/05/18 08:14:26	<i>2018/05/18 13:51:58</i>	<i>1.00</i>	40.32 \pm 3.80	
2016/09/01 16:37:55, $M = 7.0$	1993/10/06 08:22:46	1995/02/04 15:25:31	1.33	30.43 \pm 0.60	
	1996/02/29 10:55:40	2001/10/21 00:29:18	5.64	27.30 \pm 0.38	
	2002/04/20 15:52:57	2011/11/18 07:31:57	9.58	39.32 \pm 0.74	
	2013/01/01 12:33:32	2014/10/03 03:22:50	1.75	38.30 \pm 3.58	
	2015/06/05 13:27:03	2016/09/01 04:13:05	1.24	44.30 \pm 1.93	
			0.55		
	2017/04/03 18:10:48	<i>2018/08/17 04:47:03</i>	<i>1.37</i>	<i>17.45 \pm 0.70</i>	
	1997/02/11 08:25:10	2010/08/30 00:29:12	13.55	107.67 \pm 4.03	
	2010/09/03 16:35:42, $M = 7.0$			2.54	
		2013/04/19 19:20:05	2016/11/22 05:28:28	3.59	35.31 \pm 0.57
1994/09/10 10:16:22		1996/03/04 23:28:06	1.48	55.91 \pm 2.47	
1996/04/10 14:31:22		2010/09/04 07:13:19	14.40	86.19 \pm 2.25	
2012/12/07 04:36:02		2016/11/07 23:33:42	3.92	47.91 \pm 1.99	
2016/11/13 11:02:56, $M = 7.8$			1.04		
	2017/12/02 14:35:23	<i>2018/08/09 07:56:14</i>	<i>0.68</i>	22.56 \pm 0.80	
	1992/07/13 03:14:13	1993/08/08 12:20:00	1.07	14.89 \pm 3.17	
1993/08/10 00:51:52, $M = 7.0$			0.65		
	1994/04/06 04:51:06	2000/11/01 20:30:40	6.58	31.45 \pm 1.09	
	2001/06/20 21:49:26	2009/06/14 18:13:07	7.98	26.79 \pm 0.53	
	2004/08/03 22:00:32	2007/10/15 21:30:03	3.20	18.08 \pm 0.43	
	2008/02/22 11:39:03	2009/07/15 10:46:45	1.39	14.75 \pm 0.48	
	2010/01/22 20:36:41	<i>2018/07/07 06:06:22</i>	<i>8.45</i>	<i>41.62 \pm 1.28</i>	
	1994/01/24 00:05:43	2001/01/15 09:39:00	6.98	31.91 \pm 1.09	
	2001/04/04 05:10:55	2003/07/06 04:20:25	2.25	24.66 \pm 0.68	
			0.80		
	2003/08/21 12:12:50, $M = 7.2$	2004/06/20 03:51:05	2007/10/11 11:27:37	3.31	17.56 \pm 0.52
2008/01/17 01:55:11		2009/06/14 18:13:07	1.41	13.98 \pm 0.54	
2010/01/11 09:10:36		<i>2018/08/06 14:47:58</i>	<i>8.57</i>	<i>38.11 \pm 1.00</i>	
1998/09/20 07:54:01		2004/11/21 10:59:10	6.17	69.29 \pm 2.97	
			0.00		
2004/11/22 20:26:32, $M = 7.1$	2004/11/22 20:31:34	2007/02/01 12:33:48	2.19	80.55 \pm 2.72	
	2007/02/19 08:40:37	2009/07/15 10:46:45	2.40	73.00 \pm 3.21	
	2010/12/08 02:17:56	2012/01/23 04:40:42	1.13	29.14 \pm 0.68	
	2012/10/20 01:31:33	2018/08/12 02:35:12	5.81	43.89 \pm 1.35	
	1994/05/14 01:05:53	2000/11/03 01:10:45	6.48	29.18 \pm 0.97	
	2001/04/04 05:10:55	2003/08/20 09:54:31	2.38	31.61 \pm 1.02	
	2004/04/23 13:22:28	2009/05/13 00:49:59	5.05	21.95 \pm 0.61	
			0.31		
2009/07/15 09:22:29, $M = 7.8$	2009/11/04 03:17:04	<i>2018/07/20 02:41:13</i>	<i>8.71</i>	22.92 \pm 0.57	

η is in the same arbitrary units as in Fig. 10; the last periods of stability are determined as of August 21, 2018 so that their end time and estimates of $\langle \eta \rangle$ (in italics) may change in the future; the period of stability before the 1993 major earthquake is determined making use of the GeoNet Search data from 1990

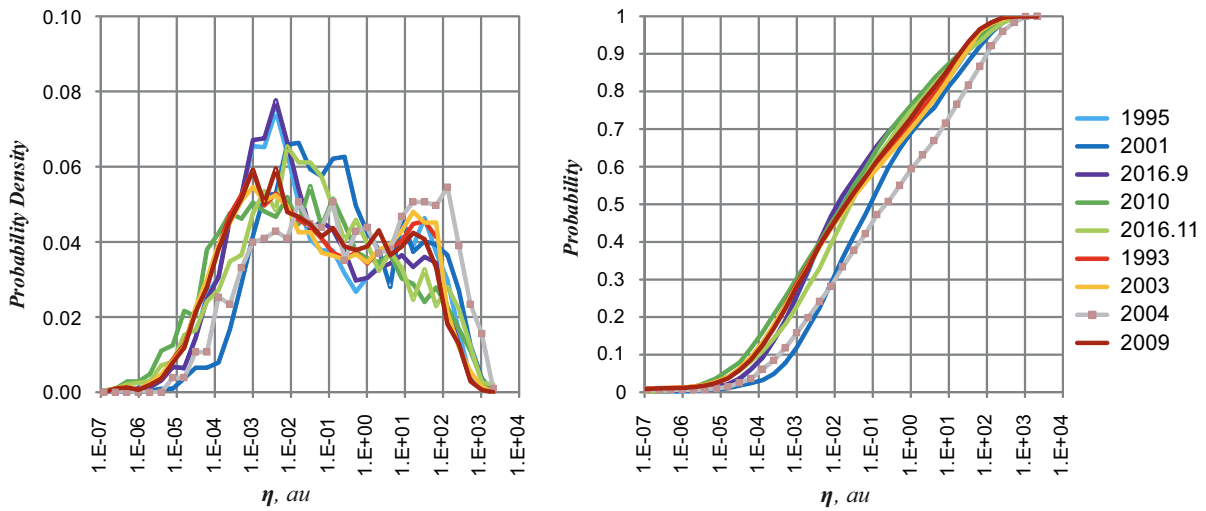


Figure 11

Empirical density (left) and cumulative (right) distribution functions of the USLE control parameter η for circles of 1° radius centered at the epicenters of the nine major earthquakes. Note the logarithmic time scale and bins exponentially increasing by factor 2

Table 7

Periods of transition of the control parameter η associated with the nine major earthquakes in New Zealand, 1993–2018

Index	Date	M_{ANSS}	Duration, days	$\langle \eta \rangle_b$	$\langle \eta \rangle_a$	$\langle \eta \rangle_a / \langle \eta \rangle_b$
a	1995/02/05 22:51:02	7.1	400	39.47	31.52	0.80
b	2001/08/21 06:51:58	7.1	395	61.04	53.97	0.88
c	2016/09/01 16:37:55	7.0	214	44.30	17.45	0.39
d	2010/09/03 16:35:42	7.0	959	107.67	35.31	0.33
e	2016/11/13 11:02:56	7.8	384	47.91	22.56	0.47
f	1993/08/10 00:51:52	7.0	239	14.89	31.45	2.11
g	2003/08/21 12:12:50	7.2	304	24.66	17.56	0.71
h	2004/11/22 20:26:32	7.1	0	69.29	80.55	1.16
i	2009/07/15 09:22:29	7.8	112	21.95	22.92	1.04

Figure 12, analogous to Fig. 6, clearly demonstrates the difference in dimensions of the two aftershock areas; compare the area of the same 721 aftershocks of the Dusky Sound earthquake of about 160 km in length with the area of the 1386 aftershocks of the Kaikōura earthquake of about 210 km in length. The 1° limit in the definition of the nearby area is quite enough for the 2009 aftershock series, but does not fit the extent of the 2016 aftershocks. Note that the aftershock area lengths based on determinations of epicenters of magnitude $M \geq 3.5$ earthquakes within 24 h after the origin time of the main shocks are about 125 and 190 km, respectively,

which is indicative of progression of the rupture process in time from the original main shock source to neighboring blocks and faults.

Figure 13, analogous to Fig. 7, shows the interevent time (τ) versus the earthquake origin time for the two samples of earthquakes at angular distance of 2.5° from the epicenters of the $M7.8$ major earthquakes. Naturally, the moving averages ($\langle \tau \rangle$) determined in the larger 2.5° circles (red lines) in advance of the origin time of the main shocks are smaller than those determined in the 1° circles (green lines). It is notable that the $\langle \tau \rangle$ curves are practically the same for about 100 days after the origin time of the Dusky Sound main

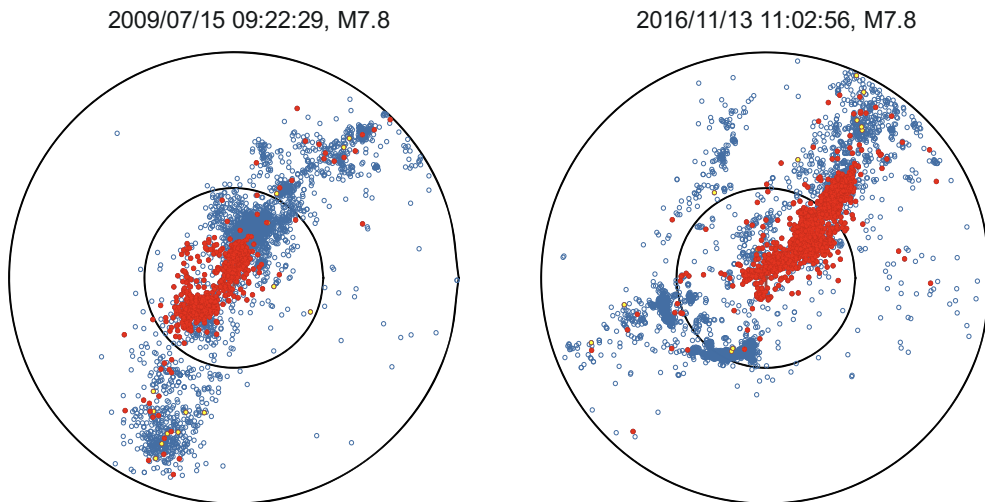


Figure 12

Epicenters of earthquakes at angular distance of 2.5° from the epicenter of the two $M7.8$ major earthquakes in New Zealand. Same as in Fig. 6

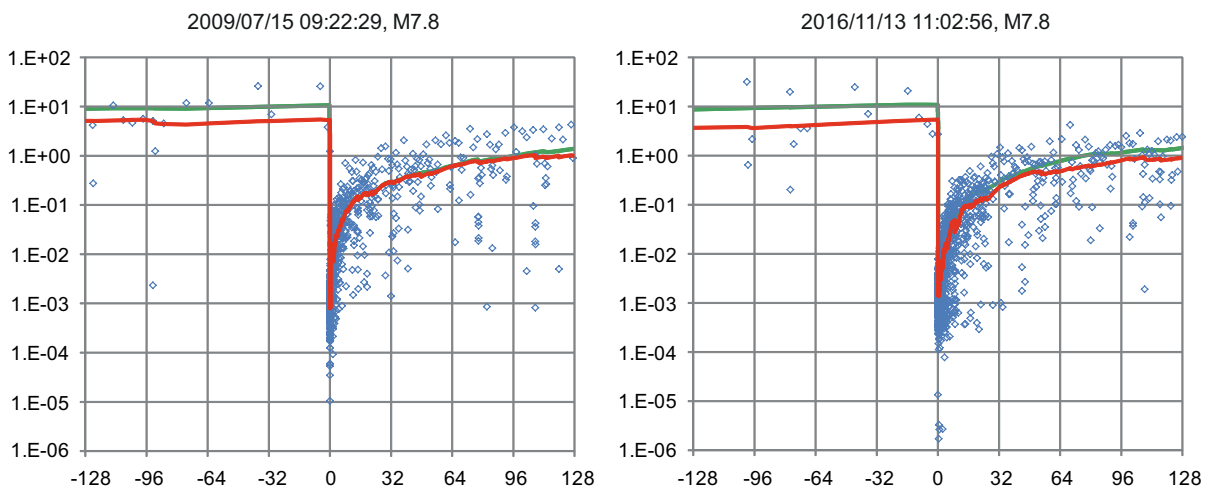


Figure 13

Interevent time τ (in days) versus earthquake origin time at angular distance of 2.5° from the epicenter of the two $M7.8$ major earthquakes in New Zealand. Notes: same as in Fig. 7; green line is 50-event moving average $\langle \tau \rangle$ for the smaller sample of earthquakes at the angular distance of 1° from the epicenter (Fig. 7)

shock, but only for a week or so in the case of the Kaikōura aftershock series; the latter can be explained by apparent redistribution of seismicity from the southwestern to northeastern part of the aftershock area outside the limit of 1° from the epicenter.

Figure 14, analogous to Fig. 10, displays the USLE control parameter η and its 50-event moving average $\langle \eta \rangle$ for the two samples of earthquakes at angular distance of 2.5° from the epicenters of the

$M7.8$ major events. Most of the time, the two red lines in Fig. 13 repeat, qualitatively, the trend lines in Fig. 10i, e. In fact, they are slightly shifted and more jerky due to the larger sample size, which implies shorter time intervals corresponding to the 50-event moving-average determinations, as well as due to additional bursts of seismicity outside the circle of 1° radius centered at the epicenter of the main shock.

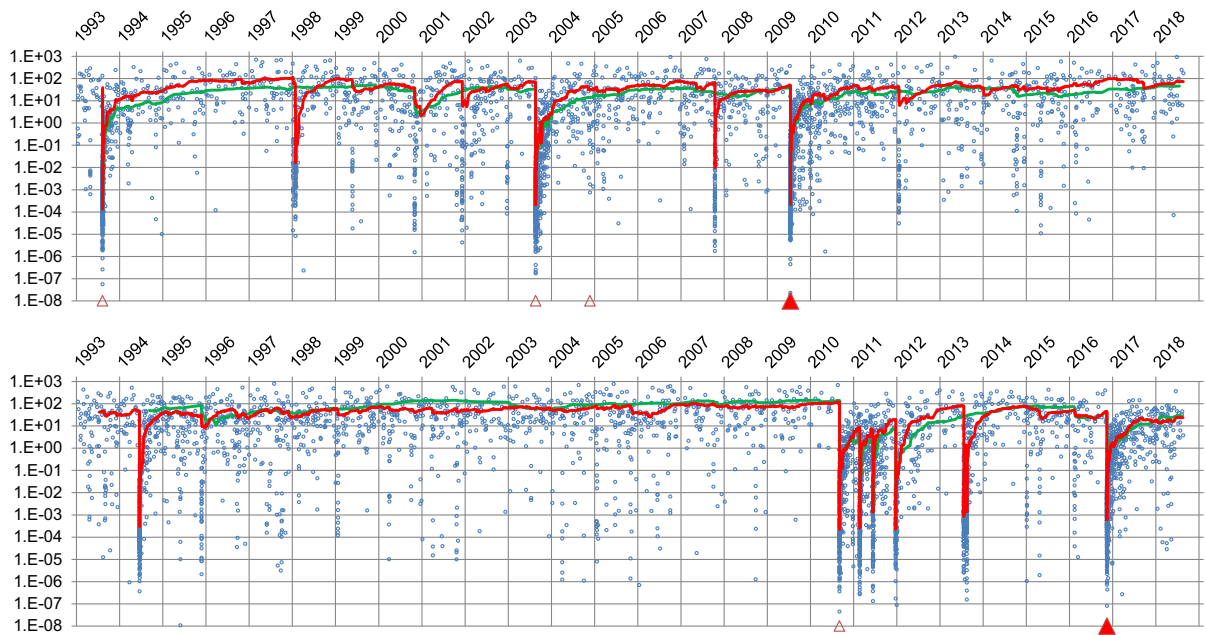


Figure 14

USLE control parameter η versus earthquake origin time at angular distance of 2.5° from the epicenters of the 15 July 2009 and 13 November 2018 major earthquakes in New Zealand. Notes: same as in Fig. 10; green line is 50-event moving average $\langle \eta \rangle$ for the smaller sample of earthquakes at angular distance of 1° from the epicenter (see Fig. 10i, e)

Table 8

Periods of stability of the control parameter η at the angular distance of 2.5° from the epicenters of the 15 July 2009 and 13 November 2018 major earthquakes in New Zealand region

Major earthquake	Start time	End time	Duration, years	Level of $\langle \eta \rangle \pm \text{err}(\langle \eta \rangle)$
	1994/04/29 16:20:11	1998/01/27 00:36:21	3.75	62.71 ± 1.88
	1998/04/06 08:56:53	2000/11/03 11:45:13	2.58	49.91 ± 1.54
	2002/01/30 05:43:12	2003/08/20 09:54:31	1.56	40.84 ± 1.23
	2004/03/29 11:54:12	2007/10/11 11:27:37	3.53	42.48 ± 0.94
	2007/12/05 23:03:11	2009/07/14 03:54:55	1.60	25.74 ± 0.70
2009/07/15 09:22:29, $M = 7.8$			0.84	
	2010/05/19 04:11:29	2012/01/20 07:28:24	1.67	33.52 ± 0.62
	2012/04/14 19:45:38	2018/08/21 07:37:39	6.35	49.99 ± 0.97
	1994/09/17 09:27:15	1995/11/27 19:09:04	1.19	30.69 ± 0.71
	1996/01/20 10:10:10	2010/08/30 00:29:12	14.61	56.18 ± 0.56
2016/11/13 11:02:56, $M = 7.8$	2012/04/19 02:32:25	2013/07/21 04:50:19	1.25	39.87 ± 2.15
	2013/11/09 12:16:02	2016/11/10 18:05:14	3.00	40.50 ± 1.01
			0.59	
	2017/06/16 23:16:00	2018/08/20 01:56:08	1.17	17.59 ± 0.23

$\langle \eta \rangle$ is in the same arbitrary units as in Figs. 10 and 13; the last periods of stability are determined as of August 21, 2018 so that their end time and estimates of $\langle \eta \rangle$ (in italics) may change in the future

Table 8, analogous to Table 6, lists the periods of stability determined for the series of earthquakes at angular distance of 2.5° from the epicenters of the two $M7.8$ major main shocks. Using the same rules of

determination applied to this larger series of earthquakes from a larger area results in the identification of a larger number of periods of stability due to additional bursts of seismicity outside the circle of 1°

radius. The 12 periods of stability identified in Table 8 are characterized by different levels of $\langle \eta \rangle$; these lie in the range from 25.74 to 62.71 and from 17.59 to 56.18, respectively. Out of the total eight cases in the two areas considered, the level of $\langle \eta \rangle$ is either higher by a factor of 1.25 than that of the previous (in two cases), lower by the factor of 1.25 (in five cases), or changes within 80–120 % (in the remaining case).

5. Conclusions

Seismic activity is evidently complex due to the variety of tectonic settings and different energy release processes. Earthquakes cluster, tracing the actual tectonic movements in space, and may swarm and/or cascade into aftershocks that readjust the nonlinear dynamical system of the naturally fractured hierarchy of blocks and faults nearby the main shock rupture (Okubo and Aki 1987; Keilis-Borok 1990). Despite more than a century of study on the redistribution of energy in seismic systems (Omori 1894; Utsu et al. 1995), the processes of seismic energy release are not yet completely understood. Recent studies of earthquake clustering on a global scale (Zaliapin and Ben-Zion 2016) conclude the existence of a spatially dependent distribution of earthquake clusters, tightly correlated with heat flow production. The observed seismic diversity appears to lie at the core of the recent debate about readjustment of a complex system of blocks and faults into a new state in advance and after a catastrophe (Ben-Zion 2008; Zaliapin et al. 2008; Mignan 2015). Notably, analysis of the interevent time distribution of aftershocks for the six strong, magnitude 6 or above earthquakes in Southern California from 1985 to 2005, in comparison with those of solar flares in certain flare-productive regions (Kossobokov et al. 2008), showed that even the same phenomenon, when observed in different periods or at different locations, is characterized by different statistics that cannot be uniformly rescaled onto a single, universal curve. Moreover, a recent study of the sequence of strong, magnitude 6 or above earthquakes in Central Italy (Kossobokov and Nekrasova 2017) confirmed this conclusion based on a comparative analysis of the interevent

time τ and USLE control parameter η determined for well-documented aftershock series from approximately the same area and even time: the epicentres of the five strong earthquakes in 1997–2016 lie within 100 km distance from each other, whereas the last three earthquakes in 2016 lie within less than 30 km distance. Our study of interevent times in the aftershock series of the major earthquakes in New Zealand does not find much variability of their best-fit model, despite the different tectonic environment of their location; the quality of either the linear or power-law best-fit approximation of τ or η is almost equally good and rather well in agreement with the classical Omori (1894) law. Note that a complex distribution of the USLE coefficients A , B , and C in the Central Mediterranean and Alpine region does not display any evident general correlation, although following a well-organized attractor in the 3-D domain of possible values (Nekrasova et al. 2011). Such kind of analysis of the A , B , and C mapping in New Zealand, as well as the two-dimensional (2-D) density distributions of the $\eta = R \times T$ components of rescaled distance and time (R , T) (Zaliapin and Ben-Zion 2016; Kossobokov and Nekrasova 2017), will be the subject of future investigation.

Thus, in the seismic sequences nearby epicenters of the major earthquakes in New Zealand, 1993–2018, we find the existence, in the long term, of different, intermittently changing local levels of rather steady seismic activity characterized by near-constant mean values of the USLE control parameter η . In the mid-term, at times of critical transitions of seismic regime, including those associated with all but one of the earthquakes of magnitude 7.0 or larger, the level of activity may switch either to higher or lower intensity of energy release, or, alternatively, remain about the same. As follows from our studies, the seismic activity at such a transition may follow different scenarios with interevent time scaling of different kinds, even when taking place at nearly the same location (Kossobokov and Nekrasova 2017). Evidently, although the results of the detailed analyses (see also Kossobokov et al. 2008) do not support the presence of universality of the impulsive seismic energy release, they provide constraints on modeling earthquake sequences that are alternative to the usually accepted oversimplified choice of behaviors

before and after the main shock. Operational monitoring of seismic regime parameters, in particular the USLE control parameter η whose mean value $\langle \eta \rangle$ determines the current state of seismicity in the area, may provide decision-makers with reliable information to improve timely local seismic hazard assessments and reduce the associated risks of disaster (Davis et al. 2012; Kossobokov et al. 2015b).

Acknowledgements

The authors acknowledge the New Zealand GeoNet project and its sponsors EQC, GNS Science, and LINZ, for providing data used in this study. Thanks to the anonymous reviewers for their comments and suggestions, which helped to clarify our claims and conclusions. The study was supported by the Russian Science Foundation (grant no. 16-17-00093).

Publisher's Note Springer Nature remains neutral with regard to jurisdictional claims in published maps and institutional affiliations.

REFERENCES

- Akaike, H. (1974). A new look at the statistical model identification. *IEEE Transactions on Automatic Control*, 19(6), 716–723. <https://doi.org/10.1109/TAC.1974.1100705>.
- Bak, P., Christensen, K., Danon, L., & Scanlon, T. (2002). Unified scaling law for earthquakes. *Physical Review Letters*, 88, 178501–178504.
- Ben-Zion, Y. (2008). Collective behavior of earthquakes and faults: Continuum-discrete transitions, progressive evolutionary changes, and different dynamic regimes. *Reviews of Geophysics*, 46(4), RG4006. <https://doi.org/10.1029/2008rg000260>.
- Christensen, K., Danon, L., Scanlon, T., & Bak, P. (2002). Unified scaling law for earthquakes. *Proceedings of the National Academy of Sciences*, 99(suppl 1), 2509–2513. <https://doi.org/10.1073/pnas.012581099>.
- ComCat (2017). ANSS Comprehensive earthquake catalog (ComCat). <https://earthquake.usgs.gov/earthquakes/search/>. Accessed 1 Jan 2018.
- Davies, G. F. (1999). *Dynamic earth: Plates, Plumes, and mantle convection*. Cambridge: Cambridge University Press.
- Davis, C., Keilis-Borok, V., Kossobokov, V., & Soloviev, A. (2012). Advance prediction of the March 11, 2011 Great East Japan Earthquake: A missed opportunity for disaster preparedness. *International Journal of Disaster Risk Reduction*, 1, 17–32. <https://doi.org/10.1016/j.ijdr.2012.03.001>.
- Di Giacomo, D., & Bormann, P. (2011). Earthquake energy. In H. Gupta (Ed.), *Encyclopedia of solid earth geophysics* (pp. 233–236). New York: Springer.
- Dobrovolsky, I. P., Zubkov, S. I., & Miachkin, V. I. (1979). Estimation of the size of earthquake preparation zones. *Pure and Applied Geophysics*, 117(5), 1025–1044. <https://doi.org/10.1007/BF00876083>.
- Fry, B., Bannister, S. C., Beavan, R. J., Bland, L., Bradley, B. A., Cox, S. C., et al. (2009). The M_w 7.6 Dusky Sound earthquake of 2009: Preliminary report. *Bulletin of the New Zealand Society for Earthquake Engineering*, 43(1), 24–40.
- Gabrielov, A., Newman, W. I., & Turcotte, D. L. (1999). An exactly soluble hierarchical clustering model: Inverse cascades, self-similarity, and scaling. *Physical Review E*, 60, 5293–5300.
- Gardner, J., & Knopoff, L. (1974). Is the sequence of earthquakes in S California with aftershocks removed Poissonian? *Bulletin of the Seismological Society of America*, 64(5), 1363–1367.
- GeoNet (2018) GeoNet quake search. <http://quakesearch.geonet.org.nz/>. Accessed 1 Jan 2018.
- Gledhill, K., Ristau, J., Reyners, M., Fry, B., & Holden, C. (2010). The Darfield (Canterbury) earthquake of September 2010: Preliminary seismological report. *Bulletin of the New Zealand National Society for Earthquake Engineering*, 43(4), 215–221.
- Goda, K., Yasuda, T., Mori, N., & Maruyama, T. (2016). New scaling relationships of earthquake source parameters for stochastic Tsunami simulation. *Coastal Engineering Journal*, 58(3), 1650010-1–1650010-40. <https://doi.org/10.1142/s0578563416500108>.
- Gutenberg, R., & Richter, C. F. (1944). Frequency of earthquakes in California. *Bulletin of the Seismological Society of America*, 34, 185–188.
- Gutenberg, B., & Richter, C. F. (1954). *Seismicity of the earth* (2nd ed.). Princeton: Princeton University Press.
- Hamling, I. J., Hreinsdóttir, S., Clark, K., Elliott, J., Liang, C., Fielding, E., et al. (2017). Complex multifault rupture during the 2016 M_w 7.8 Kaikōura earthquake, New Zealand. *Science*, 356(6334), eaam7194. <https://doi.org/10.1126/science.aam7194>.
- Harte, D., & Vere-Jones, D. (1999). Differences in coverage between the PDE and New Zealand local earthquake catalogs. *New Zealand Journal of Geology and Geophysics*, 42, 237–253.
- Kagan, Y. Y. (2003). Accuracy of modern global catalogs. *Physics of the Earth and Planetary Interiors*, 135, 173–209.
- Kaiser, A., Holden, C., Beavan, J., Beetham, D., Benites, R., Celentano, A., et al. (2012). The M_w 6.2 Christchurch earthquake of February 2011: preliminary report. *New Zealand Journal of Geology and Geophysics*, 55(1), 67–90.
- Kanamori, H., & Brodsky, E. H. (2001). The physics of earthquakes. *Physics Today*, 54, 34–40.
- Kanamori, H., & Cipar, J. J. (1974). Focal process of the great Chilean Earthquake May 22, 1960. *Physics of the Earth and Planetary Interiors*, 9(2), 128–136. [https://doi.org/10.1016/0031-9201\(74\)90029-6](https://doi.org/10.1016/0031-9201(74)90029-6).
- Keilis-Borok, V. I. (1990). The lithosphere of the Earth as a non-linear system with implications for earthquake prediction. *Reviews of Geophysics*, 28(1), 19–34.
- Kossobokov, V. G., Lepreti, F., & Carbone, V. (2008). Complexity in sequences of solar flares and earthquakes. *Pure and Applied Geophysics*, 165, 761–775. <https://doi.org/10.1007/s00024-008-0330-z>.
- Kossobokov, V. G., & Mazhkenov, S. A. (1994). On similarity in the spatial distribution of seismicity. In D. K. Chowdhury (Ed.),

- Computational seismology and geodynamics, 1* (pp. 6–15). Washington DC: AGU, The Union.
- Kossobokov, V., & Nekrasova, A. (2012). Global seismic hazard assessment program maps are erroneous. *Seismic Instruments*, 48(2), 162–170. <https://doi.org/10.3103/S0747923912020065>.
- Kossobokov, V. G., & Nekrasova, A. A. (2017). Characterizing aftershock sequences of the recent strong earthquakes in Central Italy. *Pure and Applied Geophysics*, 174, 3713–3723. <https://doi.org/10.1007/s00024-017-1624-9>.
- Kossobokov, V., Peresan, A., & Panza, G. F. (2015a). Reality check: seismic hazard models you can trust. *EOS*, 96(13), 9–11.
- Kossobokov, V., Peresan, A., & Panza, G. F. (2015b). On operational earthquake forecast and prediction problems. *Seismological Research Letters*, 86(2), 287–290. <https://doi.org/10.1785/0220140202>.
- Lay, T., Kanamori, H., Ammon, C. J., Nettles, M., Ward, S. N., Aster, R. C., et al. (2005). The great Sumatra-Andaman earthquake of 26 December 2004. *Science*, 308(5725), 1127–1133. <https://doi.org/10.1126/science.1112250>.
- Mignan, A. (2015). Modeling aftershocks as a stretched exponential relaxation. *Geophysical Research Letters*, 42, 9726–9732. <https://doi.org/10.1002/2015GL066232>.
- Nekrasova, A. K., & Kossobokov, V. G. (2005). Temporal variations in the parameters of the Unified Scaling Law for Earthquakes in the eastern part of Honshu Island (Japan). *Doklady Earth Sciences*, 405, 1352–1356.
- Nekrasova, A., Kossobokov, V. (2002). Generalizing the Gutenberg-Richter scaling law. *EOS Trans. AGU*, 83(47), Fall Meet. Suppl., Abstract NG62B-0958.
- Nekrasova, A. K., & Kossobokov, V. G. (2016). Unified scaling law for earthquakes in Crimea and Northern Caucasus. *Doklady Earth Sciences*, 470(2), 1056–1058.
- Nekrasova, A., Kossobokov, V. G., Parvez, I. A., & Tao, X. (2015). Seismic hazard and risk assessment based on the unified scaling law for earthquakes. *Acta Geodaetica et Geophysica*, 50(1), 21–37. <https://doi.org/10.1007/s40328-014-0082-4>.
- Nekrasova, A., Kossobokov, V., Peresan, A., Aoudia, A., & Panza, G. F. (2011). A multiscale application of the unified scaling law for earthquakes in the Central Mediterranean Area and Alpine Region. *Pure and Applied Geophysics*, 168, 297–327. <https://doi.org/10.1007/s00024-010-0163-4>.
- Nekrasova, A., Kossobokov, V., Peresan, A., & Magrin, A. (2014). The comparison of the NDSHA, PSHA seismic hazard maps and real seismicity for the Italian territory. *Natural Hazards*, 70(1), 629–641. <https://doi.org/10.1007/s11069-013-0832-6>.
- Okubo, P., & Aki, K. (1987). Fractal geometry in the San Andreas fault system. *Journal of Geophysical Research Atmospheres*, 92(B1), 345–356. <https://doi.org/10.1029/JB092iB01p00345>.
- Omori, F. (1894). On the after-shocks of earthquakes. *Journal of the College of Science, Imperial University of Tokyo*, 7, 111–200.
- Panza, G., Kossobokov, V. G., Peresan, A., & Nekrasova, A. (2014). Chapter 12. Why are the standard probabilistic methods of estimating seismic hazard and risks too often wrong? In M. Wyss & J. Shroder (Eds.), *Earthquake hazard, risk, and disasters* (pp. 309–357). London: Elsevier.
- Parvez, I. A., Nekrasova, A., & Kossobokov, V. (2014). Estimation of seismic hazard and risks for the Himalayas and surrounding regions based on Unified Scaling Law for Earthquakes. *Natural Hazards*, 71(1), 549–562. <https://doi.org/10.1007/s11069-013-0926-1>.
- Reyners, M., Eberhart-Phillips, D., & Martin, S. (2013). Prolonged Canterbury earthquake sequence linked to widespread weakening of strong crust. *Nature Geoscience*, 7, 34–37. <https://doi.org/10.1038/ngeo2013>.
- Simons, M., Minson, S. E., Sladen, A., Ortega, F., Jiang, J., Owen, S. E., et al. (2011). The 2011 magnitude 9.0 Tohoku-Oki earthquake: mosaicking the megathrust from seconds to centuries. *Science*, 332, 1421–1425. <https://doi.org/10.1126/science.1206731>.
- Smirnov, N. (1948). Table for estimating the goodness of fit of empirical distributions. *Annals of Mathematical Statistics*, 19, 279–281. <https://doi.org/10.1214/aoms/1177730256>.
- Stirling, M., McVerry, G., Gerstenberger, M., Litchfield, N., Van Dissen, R., Berryman, K., et al. (2012). National seismic hazard model for New Zealand: 2010 update. *Bulletin of the Seismological Society of America*, 102(4), 1514–1542. <https://doi.org/10.1785/0120110170>.
- Storcheus, A. V. (2011). Calculating the seismic energy of earthquakes and explosions. *Journal of Volcanology and Seismology*, 5, 341–350. <https://doi.org/10.1134/S0742046311050071>.
- Turcotte, D. L. (1997). *Fractals and chaos in geology and geophysics* (2nd ed.). Cambridge: Cambridge University Press.
- Utsu, T., & Ogata, Y. (1997). Statistical analysis of seismicity. In J. H. Healy, V. I. Keilis-Borok, & W. H. K. Lee (Eds.), *Algorithms for earthquake statistics and prediction* (Vol. 6, pp. 13–94). El Cerrito: IASPEI Software Library, Seismological Society of America.
- Utsu, T., Ogata, Y., & Matsu'ura, R. S. (1995). The centenary of the Omori formula for a decay law of aftershock activity. *Journal of Physics of the Earth*, 43(1), 1–33.
- Wells, D., & Coppersmith, K. (1994). New empirical relationships among magnitude, rupture length, rupture width, rupture area, and surface displacement. *Bulletin of the Seismological Society of America*, 84, 974–1002.
- Werner, M. J., & Sornette, D. (2008). Magnitude uncertainties impact seismic rate estimates, forecasts, and predictability experiments. *Journal of Geophysical Research*, 113, B08302. <https://doi.org/10.1029/2007JB005427>.
- Wyss, M., Nekrasova, A., & Kossobokov, V. (2012). Errors in expected human losses due to incorrect seismic hazard estimates. *Natural Hazards*, 62(3), 927–935. <https://doi.org/10.1007/s11069-012-0125-5>.
- Zaliapin, I., & Ben-Zion, Y. (2016). A global classification and characterization of earthquake clusters. *Geophysical Journal International*, 207, 608–634.
- Zaliapin, I., Gabrielov, A., Keilis-Borok, V., & Wong, H. (2008). Clustering analysis of seismicity and aftershock identification. *Physical Review Letters*, 101, 018501. <https://doi.org/10.1103/PhysRevLett.101.018501>.